Nonlinear behaviour of epoxy and epoxy-based nanocomposites: an integrated experimental and computational analysis

Mertol Tüfekci[a], Tuğba Baytak[b], Osman Bulut[b], İnci Pir[c], Seren Acarer Arat[d], Burak Özkal[e], Haibao Liu[f], John P. Dear[a], and Loïc Salles[g]

[a]Department of Mechanical Engineering, Imperial College London, London, UK; [b]Department of Civil Engineering, Istanbul Technical University, Maslak, Istanbul, Turkey; [c]Faculty of Mechanical Engineering, Istanbul Technical University, Beyoğlu, Turkey; [d]Department of Environmental Engineering, Istanbul University-Cerrahpaşa, Istanbul, Turkey; [e]Department of Metallurgical and Materials Engineering, Istanbul Technical University, Maslak, Istanbul, Turkey; [f]School of Engineering and Materials Science, Queen Mary University of London, London, UK; [g]Department of Aerospace and Mechanical Engineering, University of Liège, Liège, Belgium

ABSTRACT

The focus of this study is on the nonlinear mechanical properties of epoxy and epoxy-based nanocomposites, exploring frequency and strain amplitude dependency. Nanocomposite samples of epoxy are reinforced with fumed silica (FS), halloysite nanotubes (HNT) and Albipox 1000 rubber (Evonik) nanoparticles. Considering these particles have different geometries and stiffnesses, they are expected to have significantly different influences on the mechanics of the resulting composite. To enhance the reliability of the results and to reveal the impact of nanofillers on the mechanics of the material more distinctly, the manufacturing process is designed to be the same for all the specimens within the same material groups to eliminate the effects of the manufacturing process. The comprehensive characterization process consists of Fourier-Transform InfraRed Spectroscopy (FTIR), Scanning Electron Microscopy (SEM) and Dynamic Mechanical Analysis (DMA). The DMA tests are designed so that the material properties are measured depending on the vibration frequency and strain amplitude. Finally, the characterized nonlinear dynamic properties of these nanocomposites are used as the input material properties into a numerical model. In this simulation, a cantilever beam with representative nonlinear material properties, for these nanocomposites, is created, as example and its forced response is plotted under the same levels of excitation in the frequency domain. Key effects of the different nanofillers are identified using the resonance behavior, primarily focusing on the stiffness and damping of the epoxy-based nanocomposites. These experimental and numerical procedures followed show the significant impact of the nanoparticle reinforcements on the nonlinear nature of these epoxy-based composites.

KEYWORDS

Nanocomposites; characterization; stiffness and damping; frequency and amplitude dependence; nonlinear materials

1. Introduction

The nature of the majority of modern engineering designs are often significantly nonlinear which usually root from the materials and the structural properties including intrinsic material properties, discontinuous structure in a material e.g. a composite, contacts and of course large deformations. Materials in engineering are categorized based on how they are deformed when loaded. When deformation occurs under load, then, it is important to make the distinction as to whether the material is linear or nonlinear. If the material stiffness is constant, then the material characteristics are linear, whereas if the stiffness depends on the deformation and/or the deformation rate, the material is nonlinear (Ogden 1984; M. Tüfekci et al. 2023).

The nonlinearity of material response can be expressed mathematically by material constitutive relationships (Lee et al. 2008; Sadd 2019). As a result, the function chosen to represent the nonlinear behavior becomes significant (Nguyen, Wu, and Noels 2019). Thus, there are various ways to represent the material characteristics in the literature that scientists have developed over history. The chosen function controls the characteristic of the mechanical system. Especially if other parameters such as geometry and thermal effects get involved, the nature of the system becomes even more complicated which makes the modeling even more difficult (E. Tüfekci 2001); C. Li et al. 2022). Thus, the selection of the function for the material behavior is the first and the key step of the modeling. For instance, a loaded, perfectly elastic material is supposed to return to the same resting point when the load is removed, whilst plasticity causes the material to rest at a different position/form when the load is removed (Tufekci et al. 2019). This behavior can be captured with certain types of functions.

In these constitutive equations, different material models employ different functions. These functions are selected based on the data acquired from material characterization experiments that focus on mechanical behavior under various loading scenarios (Luo and Daniel 2003). Considering polymers are usually less stiff materials compared to metallic materials, a different technique/model is necessary to predict their mechanics (M. Tüfekci et al. 2020). Hyperelasticity is based on this lower stiffness assumption as well as incompressibility (Poisson's ratio $\nu = 0.5$), depending on the load history and pseudoelastic behavior (Richards and Odegard 2010; Johlitz and Diebels 2011). A significant amount of efforts are put into the research on the analysis of hyperelastic structures, particularly their statics, dynamics and internal resonance, along with their nonlinear vibrational and bending behaviors (Khaniki et al. 2023b; Khaniki and Ghayesh 2023; Khaniki et al. 2022, Khaniki, Ghayesh, and Chin 2023a). Understanding hyperelasticity plays a critical role in designing systems with very compliant materials. However, it is important to consider the damping behavior of polymeric materials. Often, viscoelasticity modeling is employed which describes the material behavior as a combination of coupled viscous and elastic responses (Ouis 2004). With the viscous behavior, this modeling technique takes damping into account (Schapery 1969). This damping can take the form of linear viscoelasticity and/or nonlinear viscoelasticity (Bilasse, Daya, and Azrar 2010; M. Tüfekci et al. 2021).

Damping affects the whole mechanical behavior of structures in steady-state and transient situations (Johnson and Kienholz 1982). Damping is one of the most crucial properties of a vibrational system, so it needs to be predicted accurately to avoid future problems and to derive possible benefits during the design process (Crandall 1970). Adhikari reviews and explains in detail some of the most commonly used and essential damping models (Adhikari 2000). The first class of damping in terms of simplicity would be linear damping (Woodhouse 1998). Some commonly used linear damping models are the linear viscous and linear viscoelastic damping models (Lin and Zhu 2009). Viscous damping is usually better when modeling systems with a lesser degree of freedom, such as damping elements or external damping effects (Tan and Rogers 1995). For material damping, the viscoelastic material model offers much more flexible and more accurate modeling possibilities (Banks, Hu, and Kenz 2011). Linear viscoelastic damping is often

expressed using the complex modulus approach (Ouis 2004). This approach is based on adding a complex part to the Young's and shear moduli of the material.

The mathematics must also be modified to increase the accuracy in modeling the inherent damping. The calculation process of the eigenvalues and eigenvectors of viscoelastic systems are also defined in detail in previous research that can be found in the literature (Lázaro, Pérez-Aparicio, and Epstein 2012; Adhikari and Pascual 2009). These two linear damping methods are often suitable for a specific range of frequency in which they are modulated. It should be noted that these models do not precisely represent the damping behavior of the material or the structure. Although linear viscoelasticity is more accurate than viscous damping in the modeling of material damping, nonlinear viscoelasticity is even more accurate to this extent. However, it is computationally much more expensive compared to the linear theories. For nonlinear damping, the challenge is to choose the suitable functions to represent the behavior of real systems, just like the issue with the functions inserted into the constitutional equation of the materials (Krack and Gross 2019; Hu and Zhou 2022a, 2022b). Polynomials are the first type of function to represent nonlinearities. With sufficient terms, any type of function, even unknown functions, can be approximated (Xiao, Jing, and Cheng 2013). However, for some cases, there are better solutions that require less computational resources than polynomials (Karkar, Cochelin, and Vergez 2013). The selected functions can be fitted to the experimental data to determine the necessary coefficients and to fully define the functions (Schapery 1969). Another type of modeling nonlinear behavior of viscoelastic damping is to take advantage of fractional derivatives of viscoelasticity (Padovan and Sawicki 1998). The investigation of the effect of the fractional derivatives on vibrational behavior of a mechanical system can be found in literature as well (Rossikhin and Shitikova 1997). It is also possible to explain how fractional derivatives come into existence in the physical world of real materials (Torvik and Bagley 1984).

For the investigation of damping, there are different measures to interpret the effect of damping apart from the energy sink (Adhikari 2000). Free vibration behavior of a mechanical system is one of the significant phenomena where the damping behavior could be extracted by evaluating the ratios of successive peaks and the time for the vibration to fade out (Rossikhin and Shitikova 1997). Amplitude, period and phase lag between the force and displacement functions in a steady state forced vibration are also essential concepts on interpreting the damping characteristics of the systems (Krack, Bergman, and Vakakis 2016). There is also some research that analyses and evaluates the hysteresis curves of materials to obtain the damping characteristics (Amadori and Catania 2018).

Experimental approaches are generally seen as the more reliable methods for characterizing dynamic mechanical material behavior (Jordan et al. 2005). Several experimental techniques and methodologies are used for investigating nonlinear dynamic characteristics of various materials. Mace et al. propose a novel, less computationally demanding approach for damping prediction in composite laminates that offers effective predictions without needing a detailed internal structure model, aligning closely with experimental results (Mace, Taylor, and Schwingshackl 2022a). In subsequent work, they introduce a novel damping test procedure, improving on the established impact hammer testing technique for better measurement of principal loss factors in lightly damped components (Mace, Taylor, and Schwingshackl 2022b). Next, they present an innovative technique to extract modal damping properties from flat specimens, allowing for large amplitude, single harmonic, free decay damping extraction, showing promising potential for providing reliable, amplitude-dependent parameters (Mace, Taylor, and Schwingshackl 2020). Kliem et al. utilize a vibrational test setup to examine the dynamics of a cylindrical composite structure (Kliem et al. 2019). Xu and Gupta employ dynamic mechanical analysis (DMA) to determine the storage modulus at different strain rates and temperatures (X. Xu and Gupta 2018). Xu et al. use DMA to characterize the elastic properties of polymer-based nanocomposites across various strain rates and temperatures (X. Xu et al. 2019). Esmaeeli et al. design and propose a novel setup to

measure mechanical properties at high frequencies (Esmaeeli et al. 2019). Pierro and Carbone also design a vibrational test rig, using an impact hammer to extract mechanical properties and compare the results with DMA (Pierro and Carbone 2021).

There are several parameters that influences the mechanical behavior of materials. The addition of nanoparticles has a significant impact on the mechanical properties and behavior of polymeric materials (Chen et al. 2021; Parveen et al. 2020). Srivastava and Stanley et al. present studies on carbon nanotube-epoxy resin composites and glass fabric-reinforced liquid thermoplastic composites filled with cellulose microcrystals, respectively, both enhancing composite performance (Stanley et al. 2021). The stiffness of polymeric materials strongly depends on temperature, as do the damping properties (Ludwigson, Lakes, and Swan 2002). It is well-known that the stiffness of polymers decreases with increasing temperature. This becomes particularly noticeable as the material approaches and surpasses its glass transition temperature (Tg). Beyond the Tg, the polymer transitions from a glassy state to a rubbery state, significantly altering its mechanical properties. Damping initially increases until it reaches a peak and then decreases past the peak value (Lu et al. 2017). Furthermore, the stiffness and damping characteristics of materials, especially polymers, depend on environmental hygrothermal conditions (Bouadi and Sun 1990; Fuller et al. 2021; Acarer et al. 2022, 2023). Apart from the temperature and humidity/water content, among many other parameters affecting the dynamic mechanical properties of polymers and polymer-based composites, the amplitude and frequency of the exciting loads are considered the most dominant (Padovan and Sawicki 1998; Crandall 1970; Jrad, Dion, et al. 2013). Besides, previous research shows that stiffness and damping properties are independent from each other, even under the same ambient conditions (Vescovini and Bisagni 2015). For instance, the study by Xu and Li explores bio-inspired nanocomposites, balancing stiffness and damping, to exceed traditional material limits (C. Xu and Li 2023). Moreover, Jiang, et al. present a strain gradient viscoelasticity theory for polymer networks, dealing with microstructure-dependent stress (Jiang, Li, and Hu 2023).

Nanoreinforced polymer-based composites are known for their sophisticated behavior/nature, even more complex that the mechanical behavior of polymers (Thostenson, Li, and Chou 2005; Rathi et al. 2021). Therefore, the nonlinear behavior of nanocomposites attracts attention of researchers (Al-Furjan et al. 2022; Ebrahimi, Nouraei, and Dabbagh 2020). A major source of complexity is the high surface area to volume ratio of nanoparticle reinforcements, causing interphase regions with nonlinear behavior to form (Kim et al. 2017; Hao et al. 2022; Lu et al. 2021). The presence of multiple types of nanoreinforcements increases the complexity of the interphase behavior (Owais et al. 2019; Jin et al. 2022). The orientation of these reinforcements and their alignments, especially in magnetically oriented composites, significantly enhance the anisotropy in such composites (Sierra-Romero and Chen 2018). Further complexity is introduced when considering the agglomeration of reinforcing elements, such as in the case of carbon nanotubes within multi-scale hybrid nanocomposite plates (Ebrahimi, Dabbagh, and Rastgoo 2021). Particles commonly used for nanocomposites include halloysite nanotubes (HNT), carbon nanotubes (CNT), fumed silica (FS), silica and rubber nanoparticles (M. Tüfekci et al. 2021; Acarer et al. 2021; Sprenger 2020; Ozdemir et al. 2016; Odent et al. 2015). Wang et al. investigate the properties of unidirectional fibre-reinforced composites, studying how interphase properties within the representative volume element (RVE) influence overall material properties (Wang et al. 2011).

In this study, nanocomposites with epoxy matrix and various reinforcements namely, FS, HNT and rubber nanoparticles are prepared following a consistent manufacturing procedure and characterized using Fourier transform infrared spectroscopy (FTIR), scanning electron microscopy (SEM) and DMA. FTIR analyses are conducted to make sure that the chemical compositions of the matrix are not affected by any reinforcement or the manufacturing procedure. SEM shows that the nanocomposite materials are manufactured do not contain major structural flaws like agglomeration/clustering of the reinforcements and air bubbles. The DMA aims to characterize

the nonlinear dynamic mechanical properties in terms of the dynamic stiffness and loss factor employing the complex modulus approach with vibration amplitude and frequency dependence. While earlier research often limits itself to studying just one or two types of nanoparticle reinforcements, this study expands the scope by exploring a broader range of possible materials. Despite the growing interest and activity in the field of epoxy-based nanocomposites, there remains a lack of integrated research that combines both experimental and theoretical/numerical analyses. This work fills this gap by providing a holistic perspective on the nonlinear behavior of such materials, particularly highlighting the influence of different nanoparticle reinforcements. In addition, a numerical model, that includes a cantilever beam with the representative effective nonlinear material properties through the DMA tests, is developed allowing the investigation of the effects of reinforcements on the dynamics of a structure. In this model, surface functions are fitted to the acquired forced vibration data with amplitude and frequency dependence for each material. Unlike previous models that employ oversimplified functions to represent nonlinearity, this model utilizes fitted functions to the experimental data with frequency and amplitude as the free variables representing the actual nature of the material, making the predictions more realistic and applicable as frequency and amplitude are the two dominant factors that control the material nonlinearity (Jrad, Dion, et al. 2013; Jrad, Renaud, et al. 2013). Then, these functions are inserted into the stiffness term of the equation of motion (EOM) and the nonlinear frequency responses are plotted using the appropriate (pseudo-arclength) continuation method. By doing so, a numerical model is built that can represent the complicated/nonlinear nature of the material efficiently without having to deal with time domain experimenting and numerical modeling. Thus, the effects of each type of particle on the frequency response and the material nonlinearity are discussed from another perspective. Understanding the implications of different nanofillers is crucial for tailoring the mechanical and dynamic properties of epoxy-based nanocomposites to suit specific applications. This approach presented with this study could make it possible to tailor the vibrational characteristics of composite structures. The experimental and numerical methodologies presented in this research are expected to guide the stiffness and damping analysis during the design of engineering structures employing composite materials. The novelty of this study lies in its approach to the nonlinear nature of the polymer-based nanocomposites, taking advantage both experimental and theoretical/numerical methods. The integration of these methodologies, along with the consideration of several nanoparticle reinforcements with different geometric and mechanical properties and their impact on material and structural dynamics, is a step toward a more comprehensive analysis of nanocomposite materials in engineering design. The potential applications of this research span a range of fields of engineering, including aviation, where precise and advanced understanding of dynamics of composite material could enhance the design of aircraft components. In automotive and aerospace engineering, the gained understanding could lead to development of lightweight, yet durable components, improving fuel efficiency and safety. Besides, this study could guide the development of more efficient and durable wind turbine blades or vibration absorbers in the renewable energy sector. Moreover, in marine applications, such knowledge might be essential in designing structural components that can withstand challenging sea conditions while optimizing performance.

2. Manufacturing and characterisation of the materials

2.1. Material manufacturing

Three sets of nanocomposites, as well as unfilled epoxy samples, are manufactured within the scope of this study. The first set is silica particulate reinforced epoxy and the second set is HNT reinforced epoxy. For silica reinforcement, fumed nanosilica (HDK N20 Pyrogenic Silica - Fumed Silica from Wacker Silicones) was acquired. For HNT reinforcement, Nanografi was acquired.

Also, the same epoxy resin (Laminating resin MGS L 285 Hardener MGS 285 from Hexion) with aviation certification was employed. The third and final set is prepared by using Albipox 1000 by Evonik. Figure 1 and Table 1 summarize the information related to the reinforcing particle geometries.

2.1.1. Unreinforced epoxy

The epoxy components (Laminating resin MGS L 285 Hardener MGS 285) with aviation certificates are purchased from Hexion.The resin and hardener components of epoxy are mixed slowly for 5 min at room temperature and then the mixture is cast into the mold. To prevent any bubbles in the material, which remain from the mixing process, the molded cast is put into a vacuum for 2 h. After the hardening accelerates, the mold is kept at room temperature and in atmospheric conditions for 22 h. Following that, the mold with hardened resin is post-cured at 60° C for 15 h.

2.1.2. Fumed silica and halloysite nanotube-reinforced epoxy

First, the nanoparticles are held in the furnace at 60° C for 8 h to minimize the interparticular humidity they contain. The particles are added to the resin and mechanically mixed with an electromagnetic mixer at 100 rpm at 50° C for 2 h. Then, the mixture is homogenized with ultrasonic homogenization with the temperature control that stops the homogenization when the temperature reaches 60° C to avoid overheating. This means the particles are dispersed in the epoxy resin without adding the hardener. Following mixing the particles into the resin, the mixture is put into a vacuum chamber for degassing for 1 h. Later, the hardener is added and mixed slowly for 10 min. Then the blend is cast into the mold for curing at room temperature into the vacuum chamber for 2 h. Then, the cast is left in the ambient conditions for 22 more hours. Post-curing is done the same way as the plain epoxy at 60° C for 15 h.

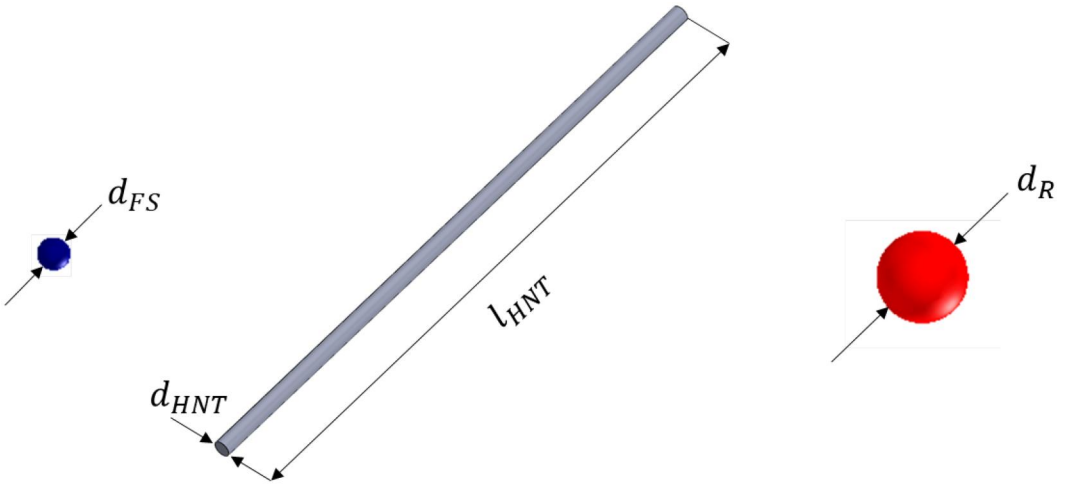

Figure 1. Representation of the particle geometries used as reinforcements (images are not to scale).

Table 1. Particle reinforcements and their dimensions.

Material groups	Diameter	Length
FS	$d_{FS} = 12$ nm	–
HNT	$d_{HNT} = 30 - 70$ nm	$l_{HNT} = 1 - 3$ µm
Rubber (Albipox 1000)	$d_R = 500 - 1000$ nm	–

The material groups are categorized based on the compositions, namely, reinforcement types and the amounts of reinforcements put in the epoxy. There are three groups of reinforced composites. The first group has silica (average diameter: 12 nm), the second has HNT (range of diameter: 30–70 nm range of length: 1–3 μm) as reinforcements. Based on the mass fractions of reinforcements, there are four groups with $0.5\%, 1\%, 1.5\%$ and 2%. Combining these, eight material groups are generated and investigated within the scope of this study. These manufactured material groups and their contents are summarized in Table 2.

2.1.3. Rubber (Albipox 1000)-added epoxy

Manufacturing of these composites contains fewer steps than the ones with HNT and silica. Since Albipox 1000 (originally contains 40% in mass rubber particles with diameters 500–1000 *nm*) is already a homogeneous mixture, there is no need to use the ultrasonic homogenization. This mixture is blended with epoxy to achieve the required reinforcement mass fractions. Then, the mixture is mechanically stirred with the electromagnetic mixer at 60° C at 100 rpm for 4 h. Following that, the mixtures are degassed in a vacuum chamber for 1 h. Afterwards, the hardener is added and mixed slowly for 5 min. Finally, the mixture is molded and put into the vacuum chamber for degassing for 2 h. Then, the mixture is left in the ambient conditions for 22 h and post-cured at 60° C for 15 h.

The categorization of the material groups are done in the same way as described in the previous section. Albipox 1000 is to be named as the reinforcement based material groups. The reinforcement mass fractions are arranged to be 5%, 10% and 15%. This material group and its material compositions are presented in Table 3.

The mold and some of the samples are displayed in Fig. 2.

2.2. Material characterisation

2.2.1. Fourier transform infrared spectroscopy

Fourier transform infrared spectroscopy (FTIR) is a powerful standardized technique to identify and quantify molecular constituents within a material by measuring the wavelengths and intensities of absorbed infrared light. It offers a quick and nondestructive way to determine the chemical bonds and molecular structures in both organic and inorganic compounds. FTIR analyses in the mid-infrared spectrum (MIR-between 4000–650 cm^{-1}), where the most important peaks related to the polymeric matrix are expected, investigate the chemical groups that are on the surface of the nanocomposite samples. Thus, they are performed to examine the chemical

Table 2. Material compositions of the nanocomposite sample groups (mass is measured in g).

	Matrix mass [g]		Reinforcement mass [g]	
Mass fractions (m_f)	Epoxy resin	Hardener	FS	HNT
0.005	85.29	34.11	0.60	0.60
0.01	84.86	33.94	1.20	1.20
0.015	84.43	33.77	1.80	1.80
0.02	84.00	33.60	2.40	2.40

Table 3. Material compositions of the nanocomposite sample groups provided by Evonik (mass is measured in g).

	Matrix mass [g]		Reinforcement mass [g]
Mass fractions (m_f)	Epoxy resin	Hardener	Albipox 1000
0.05	72.43	32.57	15.00
0.1	59.14	30.86	30.00
0.15	45.86	29.14	45.00

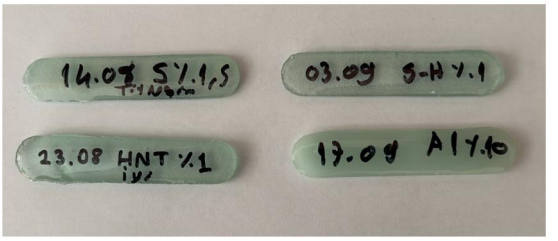

Figure 2. Manufactured samples of unreinforced epoxy and nanocomposites.

composition of the manufactured materials. This aims to ensure all the changes in the mechanical properties are purely due to the presence of the reinforcing phases.

2.2.2. Scanning electron microscopy

Scanning electron microscopy (SEM) is a visualization/imaging method using electron beams instead of light to produce detailed high-resolution images of samples. It provides a depth of focus and the capability to produce three-dimensional-like images of the surface topography and morphology of materials. Particularly useful for investigating the distribution and orientation of nanofillers within polymer matrices and possible material flaws, SEM is essential in understanding the interfacial interactions and possible agglomeration of particles in the matrix. SEM is conducted (with an SEM, FEI Quanta Feg 250) to visualize the morphology of the manufactured epoxy-based nanocomposites. Thus, the uniform dispersion of the reinforcing particles can be confirmed. The existence of any material flaws or irregularities can be significantly change the material behavior since the mechanics of the materials are mainly controlled by their internal structures. Before obtaining the SEM images of the unreinforced and reinforced epoxy samples are made conductive by coating with gold/palladium and then SEM views are obtained at 20 kV.

2.2.3. Dynamic mechanical analysis

Dynamic Mechanical Analysis (DMA) is an experimental procedure that reveals mechanical properties of materials. By subjecting material samples to a predefined stress and monitoring the resultant strain, DMA is capable of providing detailed information on the mechanics of materials. This technique offers an in-depth understanding of how materials respond under varying frequencies, temperatures and deformation modes, making it crucial for characterizing the dynamic behavior of materials particularly polymer composites. In the context as one of the most standardized methods, DMA is employed to characterize the dynamic properties of the manufactured epoxy-based nanocomposites. DMA is performed on a beam sample of the sizes 70 mm by 10 mm by 3 mm using the dual cantilever fixture on a TA DMA Q800. The dual cantilever beam configuration ensures that the required level of stiffness is achieved even with compliant materials such as these nanocomposites. The clamps at both ends of the beam sample are tightened each with two screws with 0.9 N m (8 in – lbs) standardized torque. Hence, the friction at the beam-clamp interfaces does not contribute significantly to the measured damping data. That means, the beam and the clamps stay in the full-stick regime. The test is conducted by exciting the beam sample from the middle harmonically with certain displacement amplitude and frequency. The excitation frequency goes up to 150 Hz while the strain amplitude for the beams go up to 0.1%. During the test, the force response and the displacements are used to calculate the dynamic modulus of the material. As the measures of stiffness and damping, storage modulus and loss factor are chosen. It is also important to note that all the tests are conducted multiple times for each set of samples to ensure repeatability and under constant room temperature considering these materials are temperature sensitive Feng and Guo 2016). To avoid heating of the sample

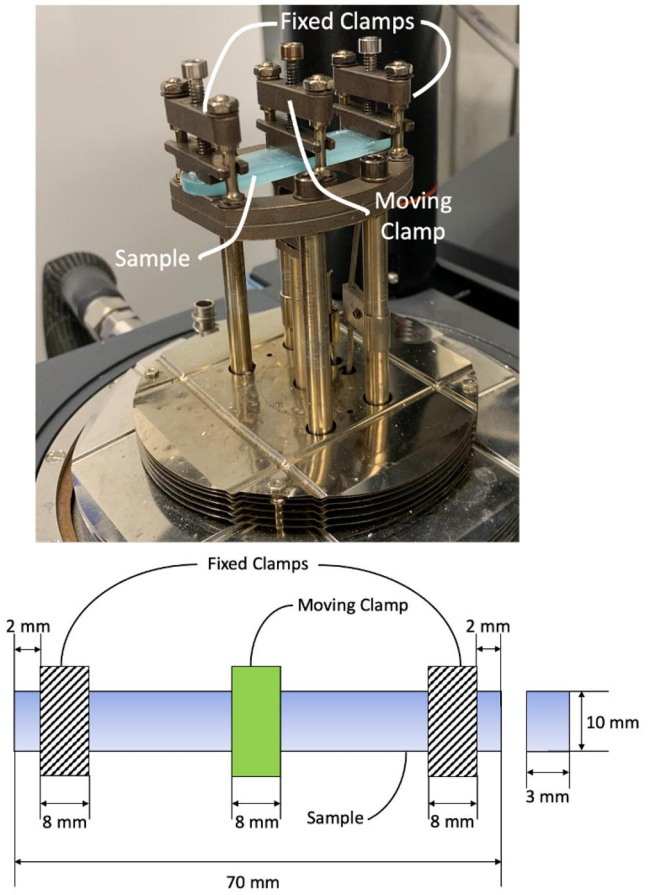

Figure 3. DMA test setup with a sample with the dual cantilever fixture configuration and the dimensions of a standard sample.

due to the deformations it is subjected to, the samples are kept idle in tha DMA chamber under the controlled room temperature for five minutes before and in between the runs. It is also important to note that the experiments are done multiple times with at least three runs to yield consistent data sets, so the repeatability of these experiments can be assessed. The DMA setup is shown in Fig. 3.

3. Forced vibration of nanocomposite elastic beams with material nonlinearity

3.1. Formulation of the cantilever beam model

To serve as an example and a model to compare the variety of nonlinearities caused by the reinforcements, a cantilever Euler–Bernoulli beam case is selected, which is excited from its free end (displayed in Fig. 4) around its first bending mode. The beam has a rectangular cross-section (width $b = 80\,\text{mm}$, height $h = 12\,\text{mm}$ and length $L = 160\,\text{mm}$) and is assumed to be made of the nonlinear nanocomposite materials manufactured and characterized within the scope of this study. Considering the excitation is mono-harmonic and only the first bending mode is of interest, the beam can be reduced to a single degree of freedom (SDOF) system as shown in Fig. 5 by calculating and using the equivalent mass, stiffness and consequently damping properties.

These equivalent stiffness/damping properties are then expressed as $k_{equivalent} = 3EI/L^3$ while the equivalent mass can be written as $m_{equivalent} = (33m_{beam})/140$. The dynamic properties

extracted as a result of the DMA tests are included within the stiffness and damping expressions as polynomial functions with the frequency, (ω) and amplitude, (X_0), dependence. To integrate this into the typical EOM of an SDOF system with a viscous damper, the following steps can be taken. From each material group (reinforcement type) the most distinctive ones compared to epoxy are selected regarding both stiffness and damping properties to make the effects of the different particles more obvious in the results. The selected materials are shown in Table 4. First, the EOM of the system can be written as in Eqs. (1) and (2) considering the viscous damper and dynamic modulus approaches separately:

$$k(X_0, \omega)y + c(X_0, \omega)\dot{y} + m\ddot{y} = F(t) \tag{1}$$

$$k^*(X_0, \omega)y + m\ddot{y} = F(t) \tag{2}$$

Here, t indicates time and y is the coordinate of the point of interest. Furthermore, k denotes the stiffness, c damping, m the mass of the SDOF system and $F(t)$ the excitation force, whilst k^*

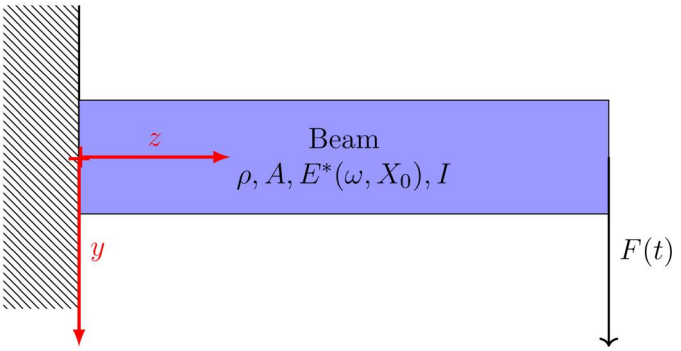

Figure 4. Cantilever Euler–Bernoulli beam system example.

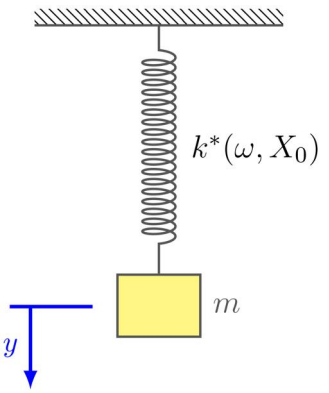

Figure 5. Reduced mechanical system with a single degree of freedom.

Table 4. Selection of the most distinctive material samples from each material group for the nonlinear vibration calculations.

Material groups	Inclusion content
FS	1%
HNT	1%
Rubber (Albipox 1000)	15%

expresses the complex dynamic stiffness. The dynamic stiffness possesses two parts, as shown in Eq. (3), the real and complex parts, thus, it is also called complex stiffness:

$$k^*(X_0,\omega) = k'(X_0,\omega)(1 + i\eta(X_0,\omega)) \tag{3}$$

i is the complex number, k', the coefficient of the real part, is responsible for the elastic potential energy storage, whereas η, the loss factor, is the coefficient of the complex part and it is the concept that leads to damping. This also explains why η stands for the loss factor.

Next, assuming a typical solution, as shown in Eq. (4), for the EOM, the response of the SDOF system is modeled:

$$x(t) = X_0 e^{(i\omega t)} \tag{4}$$

Knowing these two expressions in Eqs. (1) and (2) represent the same system, it is possible to state that they are supposed to be identical. Taking advantage of this equality, one can express the viscous damping in terms of the loss factor. This expression is presented in Eq. (5):

$$c(X_0,\omega) = \frac{k'(X_0,\omega)\eta(X_0,\omega)}{\omega} \tag{5}$$

As mentioned earlier, the stiffness of the SDOF system is obtained by calculating the equivalent stiffness of the cantilever beam excited at its tip with a concentrated force. Thus, the relation of the dynamic stiffness, which, again, depends on the amplitude and the frequency of the vibration motion, to the dynamic modulus of elasticity (E^*) is given below, in Eq. (6):

$$k^* = k^*(X_0,\omega) = \frac{3E^*(X_0,\omega)I_x}{L^3} \tag{6}$$

Here, L is the beam's length and I_x is the area moment of inertia of the cross-section of the beam. Similarly, the equivalent mass, which is a constant unlike the stiffness term, should also be presented as in Eq. (7):

$$m_{equivalent} = m_{beam}\frac{33}{140} = \rho AL\frac{33}{140} \tag{7}$$

where $m_{equivalent}$ denotes the equivalent mass and m_{beam} is the actual mass of the beam. The mass of a constant cross-sectioned beam can be expressed in terms of the density, ρ, cross-sectional area, A and the length of the beam, L.

Similar to the dynamic stiffness, the dynamic modulus of elasticity should also be formulated, as in Eq. (8):

$$E^*(X_0,\omega) = E'(X_0,\omega)(1 + i\eta(X_0,\omega)) \tag{8}$$

In the expression of the dynamic modulus of elasticity, the complex part is there to preserve the nature of the dynamic stiffness, considering that the equivalent stiffness only depends on one material property which is the modulus of elasticity. The equivalent stiffness depends on all the other parameters, which are geometric properties.

Plugging in the relation between the dynamic stiffness and the beam properties (Eqs. (6) and (8)) into the EOM with the dynamic stiffness approach in Eq. (2), the final form of the EOM is derived which is presented in Eq. (9):

$$\frac{3E'(X_0,\omega)(1 + i\eta(X_0,\omega))I_x}{L^3}y + m\ddot{y} = F(t) \tag{9}$$

Transforming the assumed solution in Eq. (4) using sine and cosine functions, the solution assumed becomes as in Eq. (10):

$$x(t) = C_1\cos(\omega t) + C_2\sin(\omega t) \tag{10}$$

C_1 and C_2 here denote the unknowns of the assumed solution function.

Then, the differential EOM is transformed into a set of two algebraic equations as shown in Eq. (11):

$$k^* C_1 - \omega^2 m C_1 = F_0 \tag{11a}$$

$$k^* C_2 - \omega^2 m C_2 = 0 \tag{11b}$$

The vibration amplitude, X_0 can be expressed in terms of the unknown coefficients of the assumed function, which leads to Eq. (12):

$$X_0 = \sqrt{C_1^2 + C_2^2} \tag{12}$$

Finally, remembering that the DMA tests characterize the material properties based on the strain amplitudes, the strain-load relation, given in Eq. (13), for a cantilever Euler–Bernoulli beam is used to convert the DMA data into a usable form in the model formulated in this section:

$$\epsilon = \frac{FLh}{2I_x E} \tag{13}$$

Here, h denotes the beam thickness and E is the modulus of elasticity of the beam material.

The final set of equations are solved numerically in frequency domain taking advantage of the pseudo-arclength continuation method which is explained briefly in the following subsection.

3.2. Pseudo-arclength continuation method

The pseudo-arclength continuation method is numerical technique employed to trace equilibrium paths in nonlinear systems, particularly in problems where standard continuation methods face difficulties due to turning points or limit points on the bifurcation diagram.

Given a nonlinear system of equations defined by:

$$\mathbf{F}(\mathbf{x}, \lambda) = 0, \tag{14}$$

where $\mathbf{x}$ represents the solution vector and λ is a bifurcation or control parameter, the objective is to compute the solution curve $C : \lambda \mapsto \mathbf{x}(\lambda)$.

For the pseudo-arclength approach, an orthogonal predictor-corrector strategy is employed. The predictor approximates the next solution point on the curve, whilst the corrector refines this approximation until the desired accuracy is achieved. The core idea is to extend the system by introducing an additional constraint that maintains an almost constant arc length between consecutive points on the solution curve:

$$s^2 - |\mathbf{x}_{i+1} - \mathbf{x}_i|^2 - (\lambda_{i+1} - \lambda_i)^2 = 0, \tag{15}$$

where s is the pseudo-arclength step size and $\mathbf{x}_i, \lambda_i$ are the current solution and parameter values, respectively.

This formulation ensures that the continuation can proceed past turning or limit points where the tangent to the curve becomes vertical, a situation that often poses challenges for standard methods.

By combining the original system of equations with the pseudo-arclength constraint, a new augmented system is formed:

$$\begin{bmatrix} \mathbf{F}(\mathbf{x}, \lambda) \\ s^2 - |\mathbf{x}_{i+1} - \mathbf{x}_i|^2 - (\lambda_{i+1} - \lambda_i)^2 \end{bmatrix} = 0. \tag{16}$$

This augmented system can then be solved using standard iterative techniques like Newton's method. The pseudo-arclength continuation has been found particularly beneficial in tracing nonlinear frequency response curves, where the presence of resonance peaks and nonlinear phenomena can cause abrupt changes in system response.

Even though the pseudo-arclength continuation method is a well-known method, the model that this continuation method is applied to is proposed by this research. The DMA experiments are performed to explore the material behavior against varying vibration amplitude and frequency, simplifying the mathematical load on the computations by making it possible to work directly in the frequency domain without requiring any transformation from time domain calculations and also without requiring any time domain experimentation. Meanwhile, the model remains representative of the actual material behavior as the data is acquired through experiments.

4. Results and discussions

4.1. Material characterisation

4.1.1. Fourier transform infrared spectroscopy

In the unreinforced epoxy, peaks occur at 2957, 2916, 2848, 1462, 1244, 826, 730 and 719 cm^{-1} as given in Table 5. The peak at 2957 cm^{-1} corresponds to the asymmetric vibration of CH_3. While the peaks at 2916 and 2848 cm^{-1} correspond to C–H stretching vibrations, the peak at 1462 cm^{-1} corresponds to the C–H bending vibration of the methylene group. The peaks at 1244 and 826 cm^{-1} can be associated with the C–H stretching vibration and the C=C bending vibration of the aromatic structure, respectively. The peaks at 730 and 719 cm^{-1} occur due to the C–H bending vibration González, Cabanelas, and Baselga 2012; Maity et al. 2008).

The spectra obtained from the FTIR analyses performed on FS-reinforced epoxy samples are presented in Fig. 6(a). With the addition of FS to the epoxy resin, the new peaks occurring at 1080, 1037 and 970 cm^{-1} prove the presence of FS in the epoxy. The peaks at 1080 and 1037 cm^{-1} can be explained with the asymmetric stretching or bending vibrations of Si–O–Si and Si–O bonds Kuzielová et al. 2021; K. M. Li et al. 2014), respectively, while the peaks at 970 cm^{-1} can be attributed to the Si–OH vibration K. M. Li et al. 2014; Shokri, Firouzjah, and Hosseini 2009; Singh Kashyap et al. 2021).

Fig. 6(b) shows the FTIR results of HNT-reinforced epoxy composites. With HNT additive to epoxy, the water in the interlayer of HNT can be identified by the bending vibration peak seen at 1634 cm^{-1} Liu et al. 2019; Sadjadi, Heravi, and Daraie 2017). The peak corresponding to 1032 cm^{-1} can be attributed to the $Si - O$ stretching vibration Berahman et al. 2016; Barot, Rawtani, and Kulkarni 2020). The large peak of O–H stretching in the range of 3200–3600 cm^{-1} in the 0.5% HNT additive may be due to some impurities in the material. The Al bonds in the HNT's structure do not appear in the plots since it is expected to appear around 400 cm^{-1}, which falls out of the bounds of the investigated spectra.

In the FTIR spectra of rubber (Albipox 1000)-reinforced epoxy composites are shown in Fig. 6(c). The results of 10% rubber (Albipox 1000) added epoxy, the peaks in the range of 3200–3600 cm^{-1}

Table 5. Peaks appearing on FTIR spectrum for epoxy.

Wave number [cm^{-1}]	Vibration type
2957	CH_3 asymmetric
2916	C–H stretching
2848	C–H stretching
1462	C–H bending
1244	C–O stretching
826	C=C bending
730	C–H bending
719	C–H bending

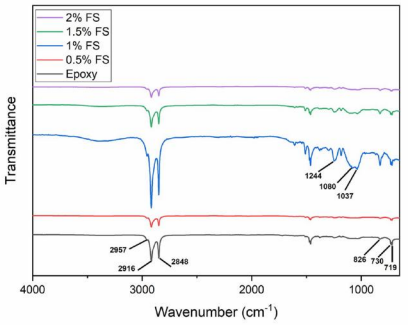

(a) FTIR spectra of FS-reinforced epoxy nanocomposites.

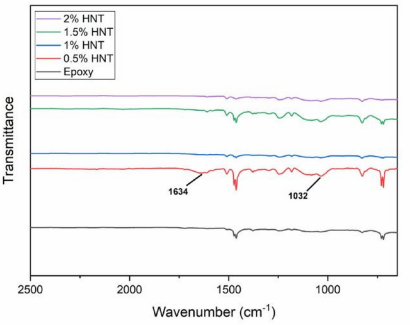

(b) FTIR spectra of HNT-reinforced epoxy nanocomposites.

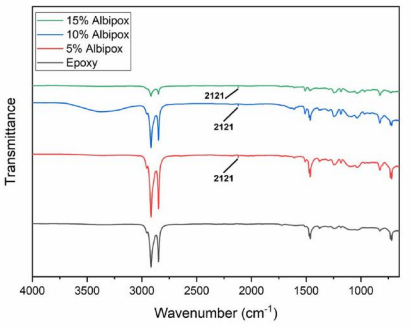

(c) FTIR spectra of rubber (Albipox 1000)-reinforced epoxy nanocomposites.

Figure 6. FTIR spectra of the manufactured epoxy and the nanocomposites (the data of the pure epoxy sample is plotted with the black (bottom) line.).

correspond to the O–H stretching vibration caused by the wide peak water. No such impurities are found in the 5% and 15% Albipox 1000 additives. With the addition of Albipox 1000, the base resin of which is DGEBA, the peaks between 2957–2848 can be attributed to the C–H stretching vibrations in CH_2 and the aromatic and aliphatic C–H stretching vibrations. The peaks occurring at 1510, 1036 and 830 cm^{-1} show the aromatic C–C stretch, the ether C–O–C stretching and the C–O stretching of the oxirane group, respectively. As a result of the addition of the rubber (Albipox 1000) to the epoxy, the presence of a new peak at 2121 cm^{-1} in the spectra is clearly seen. The peak at 2121 cm^{-1}, which corresponds to the nitrile (C≡N) group of the rubber in Albipox 1000, confirms the presence of Albipox 1000 in the epoxy.

It should be pointed that FTIR characteristics of the polymer are not markedly changed for different manufacturing processes and by the addition of different nanofillers. The changes observed in the FTIR characteristics of the composites are mainly caused by the reinforcements. It is already unlikely since no chemical reactions/alterations are expected between the epoxy matrix and the reinforcing nanoparticles in the composites that are reinforced with FS and HNT. The composites containing Albipox 1000 do not display significant changes, which is initially judged to be expected considering they are provided in an epoxy-compatible polymeric dispersion.

FTIR peaks seen in the spectra, caused by the inclusion of FS, HNT, rubber (Albipox 1000) and in the epoxy, clearly demonstrate the successful incorporation of these materials into the epoxy.

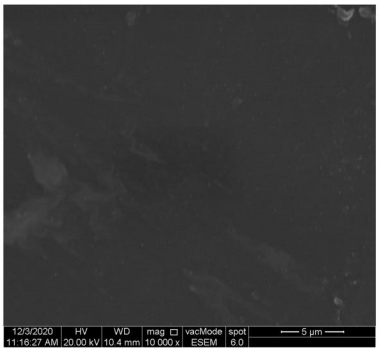

(a) SEM image of unreinforced epoxy showing a surface neither any significant material flaws nor any inclusions.

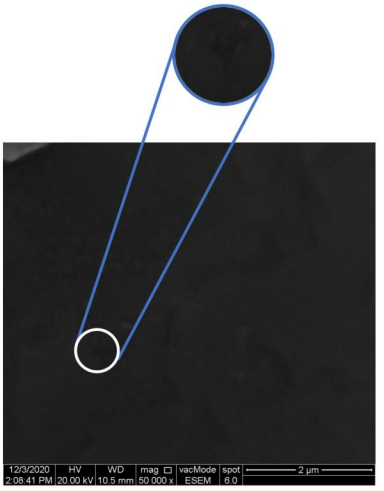

(b) SEM image of FS-reinforced epoxy nanocomposites (FS particles are the grey dots with $10-15\ nm$ diameter.).

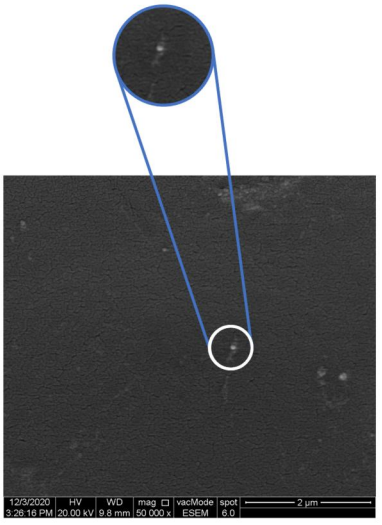

(c) SEM image of HNT-reinforced epoxy nanocomposites (HNT particles are the faint grey dots and lines with $30-70\ nm$ diameter and $1-3\ \mu m$ length.).

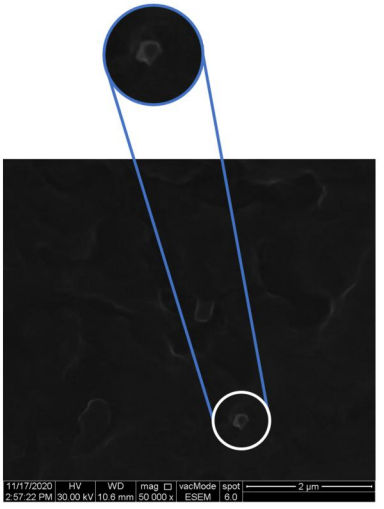

(d) SEM image of rubber (Albipox 1000)-reinforced epoxy nanocomposites (rubber particles are the grey dots within the range of $500-1000\ nm$ diameter.).

Figure 7. SEM image of the manufactured epoxy and the nanocomposites.

4.1.2. Scanning electron microscopy

Figure 7 shows SEM cross-sectional views of unreinforced epoxy and epoxy-based nanocomposite samples, respectively. The SEM surface views of the unreinforced epoxy (Fig. 7a) clearly show epoxy material has a uniform structure, with no voids formed.

In the SEM surface view of the FS-reinforced epoxy in Fig. 7(b), no material defects, voids, or cracks that reduce homogeneity are observed in the material. Also, FS showed good dispersion in the epoxy matrix. This result reveals that FS reinforcement in the epoxy does not have a tendency to agglomerate in the epoxy matrix with this manufacturing strategy and that FS has a strong

interaction with the epoxy matrix. Therefore, this indicates that the presence and properties of well-dispersed FS particles in the epoxy is effective in modifying the mechanical performance of the FS-reinforced epoxy.

With the inclusion of HNT in the epoxy matrix, a significant change occurs on the membrane surface and a cracked appearance is obtained over the entire surface structure as shown in Fig. 7(c). Another remarkable point is that the HNT-reinforced epoxy exhibits a less homogeneous surface structure compared to the FS-reinforced epoxy. Therefore, the embrittlement of the composite can be expected which has an impact on the mechanical performance of HNT-reinforced epoxy, both the performance-enhancing HNT's superior properties and more brittle behavior should be considered together.

SEM views of rubber (Albipox 1000) added epoxy samples are shown in Fig. 7(d). From Fig. 7(d), it can be pointed out that the epoxy reinforced with rubber (Albipox 1000) has a dense surface and the nanoreinforcement in rubber (Albipox 1000) is not found on the material surface. This phenomenon can be attributed to the good compatibility of rubber (Albipox 1000) and epoxy and the dispersion of the nanoreinforcement within the material structure.

4.1.3. Dynamic mechanical analysis

The results of the DMA tests are presented in this section. First of all, stress-strain plots which show the repeated loading and unloading are discussed. Stress-strain plots, which exhibit hysteresis for the FS-reinforced samples, under 1 and 150 Hz and the maximum strain amplitude of 0.12% excitation for 20 repeated cycles after reaching the steady-state, are presented in Fig. 8. These data shows that the stiffness of the materials increases with increasing FS reinforcement mass fraction. All stress-strain plots display a slight curvature and noticeable hysteresis, at these excitation frequencies and for this range of strain amplitude. The slopes of the hysteresis curves of the materials in Fig. 8(a) are found to be relatively close to the static results from the study by (M. Tüfekci et al. 2023). Moreover, there is a significant increase in stiffness of the material and dissipated energy in Fig. 8(b) compared to Fig. 8(a). The hysteresis is mainly caused by the material's intrinsic damping and not the frictional effects introduced by the clamps (Vescovini and Bisagni 2015). When friction dominates, it is expected that the curves have lower slopes or even flat tops and bottoms toward the both ends of the motion. For the stress-strain plots obtained, such a change in slope is not observed. This indicates that frictional damping either does not exist or is negligible. Also, the stress-strain plots, have forms distinctive of a viscoelastic solid, with damping properties not as high as for example viscoelastic damping seen in neoprene rubber (Chung 2001). The main reason for this is that the temperature at which these experiments are conducted, the epoxy polymer is in the glassy region, where the viscoelastic properties are not as dominant as they are in the rubbery region. These hysteresis plots also indicate that the steady-state response is achieved. Thus, it is concluded that the heating of the sample due to cyclic loading and other similar factors do not have a significant impact on the results. These data shows a settled steady-state response through the cyclic loading.

The results of the DMA tests are plotted in Figs. 9–12 which display considerable nonlinear behavior for all material types for different excitation frequency and strain amplitude.

Figure 9 shows the data acquired from the tests performed on the unreinforced epoxy samples. The variation of storage modulus of epoxy is found to be around 10% within the investigated range of strain amplitude and frequency. The storage modulus however, is not as sensitive to the strain amplitude of the vibration as it is to the excitation frequency. Increasing strain amplitude leads to a slight drop in the storage modulus whilst with increasing frequency, the storage modulus rises showing a saturation characteristic. On the other hand, the loss factor (damping) is affected more dramatically. The loss factor almost doubles as the strain amplitude and frequency increase. The loss factor of epoxy changes as a result of the viscoelasticity of the material. The variation of the material properties clearly reveal the nonlinear nature of the polymer.

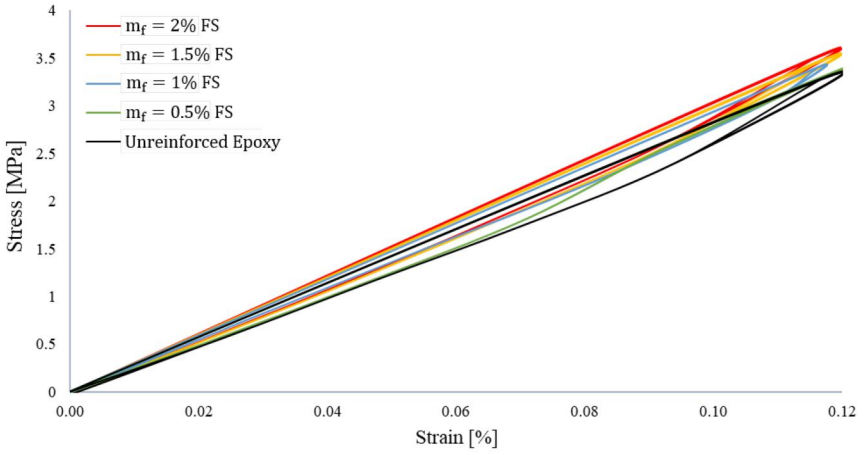

(a) Hysteresis curves (20 steady-state cycles) of the unreinforced epoxy and FS-reinforced epoxy at 1 Hz.

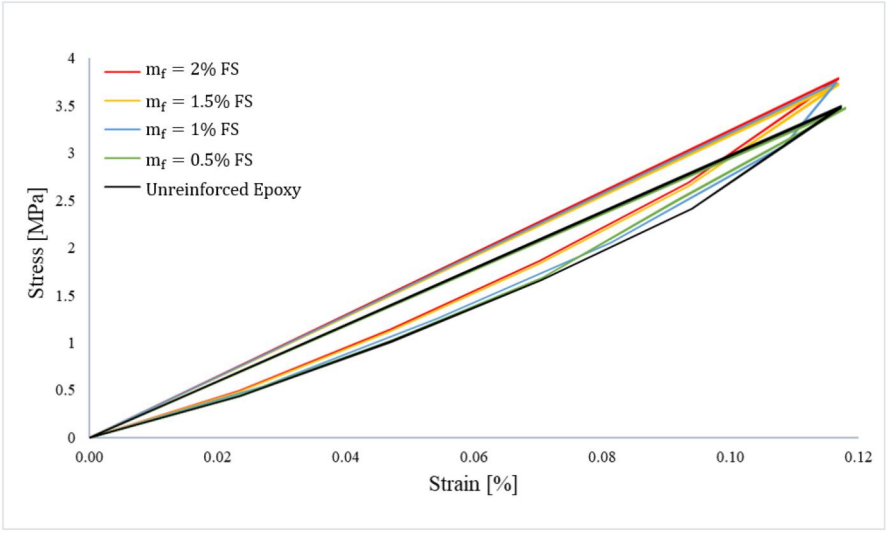

(b) Hysteresis curves (20 steady-state cycles) of the unreinforced epoxy and FS-reinforced epoxy at 150 Hz.

Figure 8. Hysteresis curves (20 steady-state cycles) of the unreinforced epoxy and FS-reinforced epoxy samples for the maximum strain amplitude of 0.12%.

The excitation frequency has a more significant effect on the loss factor compared to the strain amplitude. The results of the unreinforced epoxy are found consistent with the research published by Feng and Guo at room temperature (Feng and Guo 2016).

Considering that the loss modulus can be calculated using the storage modulus and the loss factor, only the storage modulus and the loss factor plots are presented for the next material groups. The loss modulus plots are given in A.

The results of the DMA tests conducted on FS-reinforced epoxy nanocomposites are presented in Fig. 10. The results suggest that the addition of FS up to $m_f = 1\%$ increases the storage modulus. The addition of 0.5% mass of silica stiffened the material approximately by 5% whereas it increased the damping capabilities by up to 20% compared to unreinforced epoxy. Both the storage modulus

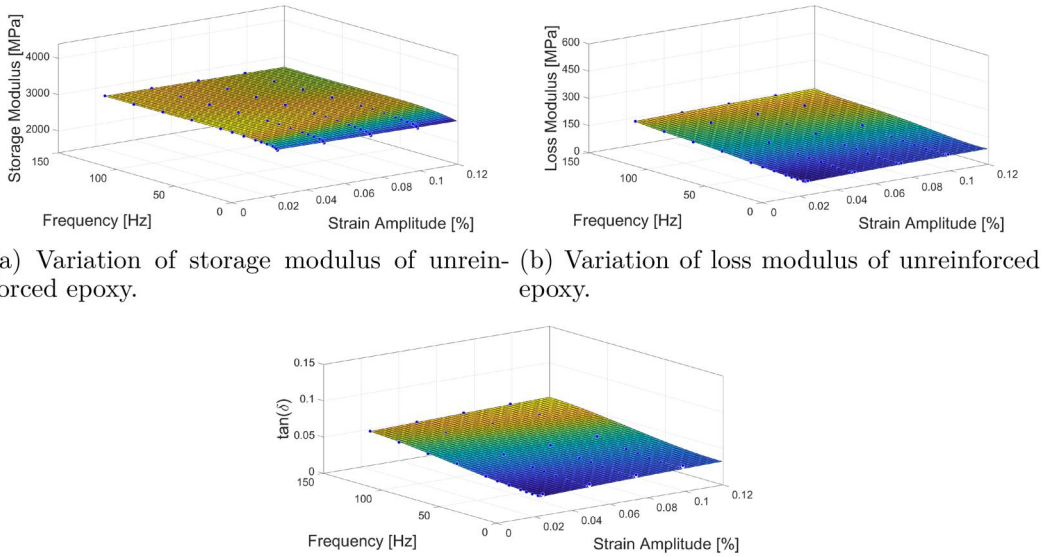

(a) Variation of storage modulus of unreinforced epoxy.

(b) Variation of loss modulus of unreinforced epoxy.

(c) Variation of loss factor of unreinforced epoxy.

Figure 9. Variation of dynamic mechanical properties of unreinforced epoxy with strain amplitude (up to 0.12%) and frequency (up to 150 Hz).

and the damping factor get their highest average values with the presence of $m_f = 1\%$ FS. This increase in the storage modulus can be explained with the stiffening effect of the particles whilst the damping is mainly related to the effect of the interfaces created between the matrix and the nanoparticles. The local plastic deformation in the matrix around the reinforcing particles is thought to be caused by the triaxial stress concentrations. There is a slight drop in the storage modulus and the loss factor with increasing amount of FS (above $m_f = 1\%$) in the epoxy resin, the FS-reinforced epoxy nanocomposites still have enhanced storage moduli and loss factors compared to the unreinforced epoxy. The drop in the storage modulus is most likely due to the increased number of stress concentration locations. These locations exhibit plastic deformation so reducing the capacity to store elastic strain energy. It is also likely that the viscoelastic properties are influenced by these plastic regions which lead to the drop in the loss modulus. At high frequency and strain amplitude, the loss factor increases and this is thought to be a localized nonlinear effect.

Figure 11 shows the results of the DMA tests performed on HNT-reinforced epoxy samples. It can be seen that the presence of HNT increases the storage modulus and the damping capability of the epoxy matrix. The storage modulus and loss factor are highest when the mass fraction of HNT is $m_f = 2\%$. HNT particles are stiffer than FS and so the increase in storage modulus is enhanced. As for the FS-reinforced samples, it is thought that the plastic deformation influences the viscoelastic properties leading to a reduction in loss modulus for $m_f = 1\%$ and higher. In all HNT-reinforced samples, a slight drop of the storage modulus is observed with increasing strain amplitude. It is thought that this fall is more significant compared to the FS-reinforced epoxy samples due to the increased magnitude of localized plastic deformations in the matrix.

The data acquired from the DMA tests of epoxy-based composites containing rubber particles is presented in Fig. 12. Unlike any other composites presented within the scope of this study, this composite displays a significant drop in storage modulus which is related to the lower stiffness of added rubber particles compared to the epoxy matrix. The general trend of the storage modulus with frequency and strain amplitude of each sample exhibits the general characteristics that other material groups also display. The storage modulus falls slightly with increasing strain amplitudes

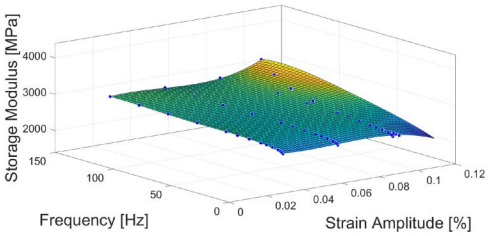

(a) Variation of storage modulus of $m_f = 0.5\%$ FS-reinforced epoxy-based nanocomposite.

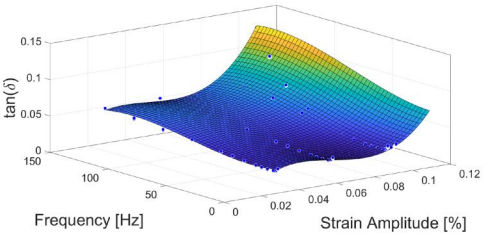

(b) Variation of loss factor of $m_f = 0.5\%$ FS-reinforced epoxy-based nanocomposite.

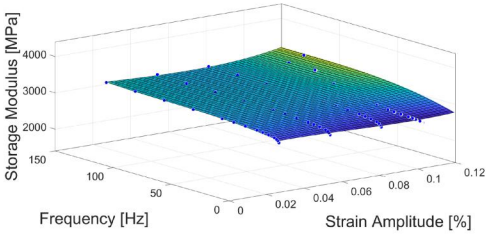

(c) Variation of storage modulus of $m_f = 1\%$ FS-reinforced epoxy-based nanocomposite.

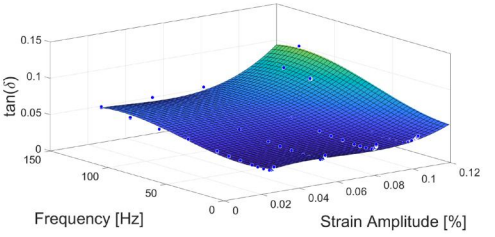

(d) Variation of loss factor of $m_f = 1\%$ FS-reinforced epoxy-based nanocomposite.

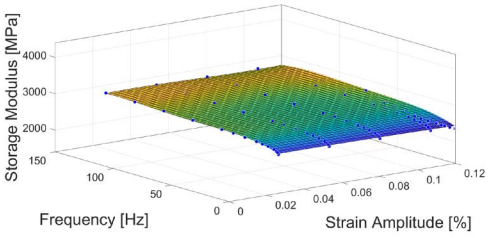

(e) Variation of storage modulus of $m_f = 1.5\%$ FS-reinforced epoxy-based nanocomposite.

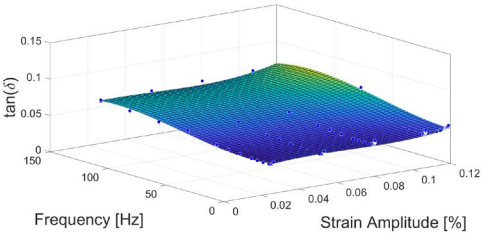

(f) Variation of loss factor of $m_f = 1.5\%$ FS-reinforced epoxy-based nanocomposite.

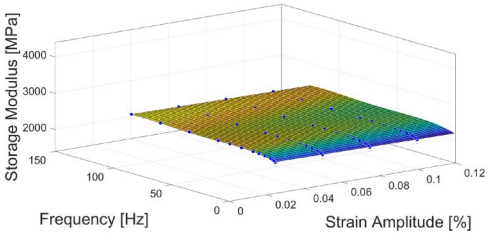

(g) Variation of storage modulus of $m_f = 2\%$ FS-reinforced epoxy-based nanocomposite.

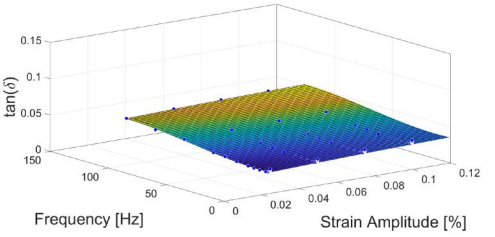

(h) Variation of loss factor of $m_f = 2\%$ FS-reinforced epoxy-based nanocomposite.

Figure 10. Variation of dynamic mechanical properties of FS-reinforced epoxy with strain amplitude (up to 0.12%) and frequency (up to 150 Hz).

and it increases significantly with increasing frequency. Meanwhile, the case with the damping of this material type is slightly more complicated. The loss factor is not strongly affected by the mass fraction of rubber. This is because the loss modulus (see Fig. A3) decreaases with increasing mass fraction of rubber in a similar way as the storage modulus. The loss factor shows a similar behavior with frequency and strain amplitude for rubber particles as for unreinforced epoxy and the other epoxy-based nanocomposites. However, the localized increase in loss factor is not present at high frequencies and high strain ampltidue for the softer rubber particles.

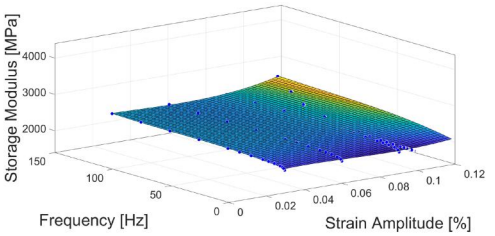

(a) Variation of storage modulus of $m_f = 0.5\%$ HNT-reinforced epoxy-based nanocomposite.

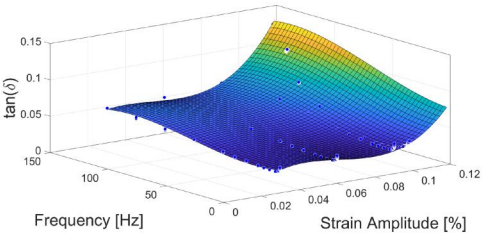

(b) Variation of loss factor of $m_f = 0.5\%$ HNT-reinforced epoxy-based nanocomposite.

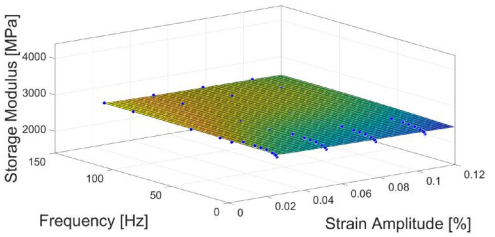

(c) Variation of storage modulus of $m_f = 1\%$ HNT-reinforced epoxy-based nanocomposite.

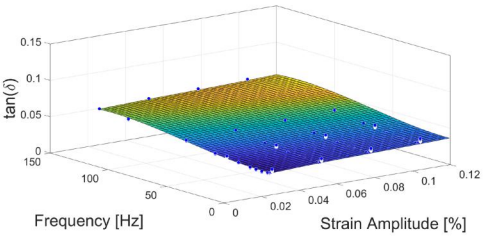

(d) Variation of loss factor of $m_f = 1\%$ HNT-reinforced epoxy-based nanocomposite.

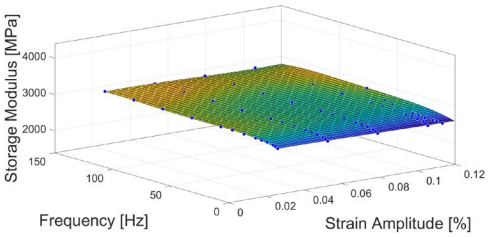

(e) Variation of storage modulus of $m_f = 1.5\%$ HNT-reinforced epoxy-based nanocomposite.

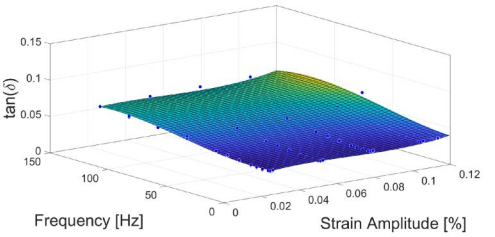

(f) Variation of loss factor of $m_f = 1.5\%$ HNT-reinforced epoxy-based nanocomposite.

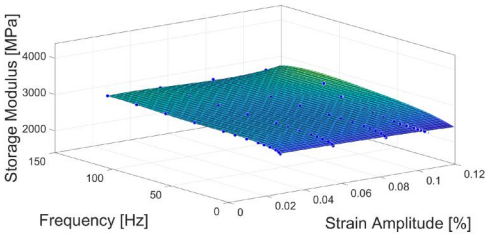

(g) Variation of storage modulus of $m_f = 2\%$ HNT-reinforced epoxy-based nanocomposite.

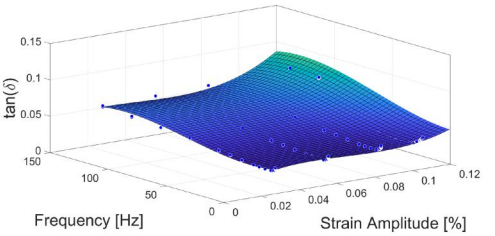

(h) Variation of loss factor of $m_f = 2\%$ HNT-reinforced epoxy-based nanocomposite.

Figure 11. Variation of dynamic mechanical properties of HNT-reinforced epoxy with strain amplitude (up to 0.12%) and frequency (up to 150 Hz).

Building on the earlier findings, the DMA results hint at some interesting ways in which different reinforcements affect epoxy-based materials. For instance, adding FS particles seems to make the epoxy stiffer, which is reflected in the storage modulus data. At the same time, these particles might also be playing a role in the observed increase in damping. This could be due to how the epoxy interacts with the nanoparticles, leading to what looks like localized deformations in the material, which is observed to be affecting the material's damping behavior.

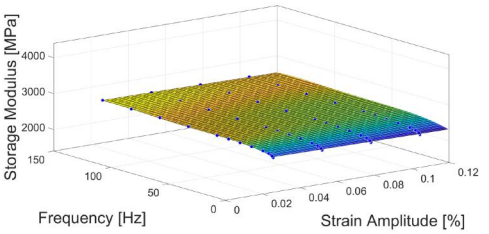

(a) Variation of storage modulus of $m_f = 5\%$ rubber (Albipox 1000)-reinforced epoxy-based nanocomposite.

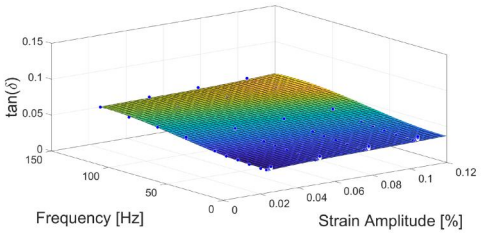

(b) Variation of loss factor of $m_f = 5\%$ rubber (Albipox 1000)-reinforced epoxy-based nanocomposite.

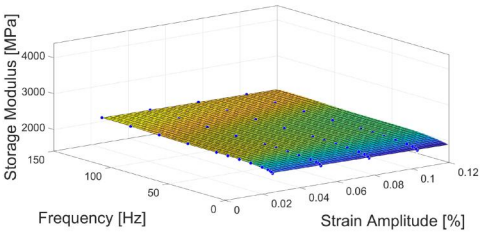

(c) Variation of storage modulus of $m_f = 10\%$ rubber (Albipox 1000)-reinforced epoxy-based nanocomposite.

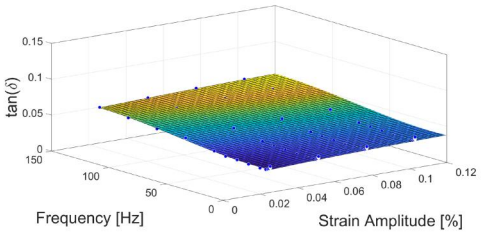

(d) Variation of loss factor of $m_f = 10\%$ rubber (Albipox 1000)-reinforced epoxy-based nanocomposite.

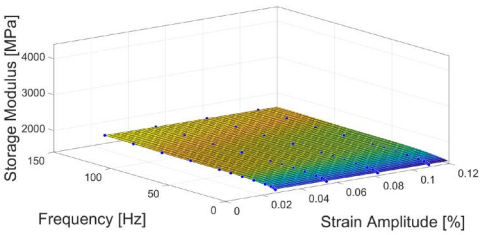

(e) Variation of storage modulus of $m_f = 15\%$ rubber (Albipox 1000)-reinforced epoxy-based nanocomposite.

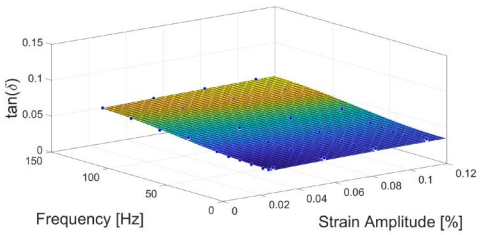

(f) Variation of loss factor of $m_f = 15\%$ rubber (Albipox 1000)-reinforced epoxy-based nanocomposite.

Figure 12. Variation of dynamic mechanical properties of rubber (Albipox 1000)-reinforced epoxy with strain amplitude (up to 0.12%) and frequency (up to 150 Hz).

In the case of HNT-reinforced samples, it seems that these particles also make the material stiffer, even more so than FS particles. Yet, similar to FS, these particles may be causing some small-scale deformations in the epoxy. These deformations are found to influencing the storage modulus, especially when more HNT is added, and also appear to contribute to the material's ability to dampen vibrations. It's worth noting that the change in storage modulus seems more noticeable when higher strain amplitudes are used, which suggests some localized changes in the material.

When rubber particles are added to the epoxy, the material appears to get less stiff, which is not surprising given that rubber is generally softer than epoxy. What's interesting here is that the damping behavior does not change in a monotonic/straightforward manner. This could be because both the storage modulus and loss modulus are decreasing somewhat in parallel. Yet, the rubber-reinforced samples display a different damping trend at higher frequencies and strain amplitudes, which could point to unique behaviors tied to rubber's specific characteristics. Therefore, each type of additive seems to offer its own set of benefits and drawbacks, providing options for fine-tuning epoxy's mechanical and damping properties.

4.2. Forced vibration of nanocomposite elastic beams with material nonlinearity

The results of the computed forced responses of the beams are plotted in Figs. 13–16. The first bending mode of the unreinforced epoxy beam is calculated as approximately 102.67 Hz. This calculation is based on the assumption of a linear model which is not continued for the rest of the calculations. Here the beam is assumed to have the constant material properties $E = 2.5GPa, \nu = 0.38$ and $\rho = 1400\text{kg/m}^3$ (which makes the structure model linear) while the vibration amplitudes are relatively small. For the beam made of unreinforced epoxy under the excitation force amplitude of $2N$, the behavior is found to be linear even with the material nonlinearity as shown in Fig. 13. Thus, the frequency that corresponds to the peak displacement amplitude for each

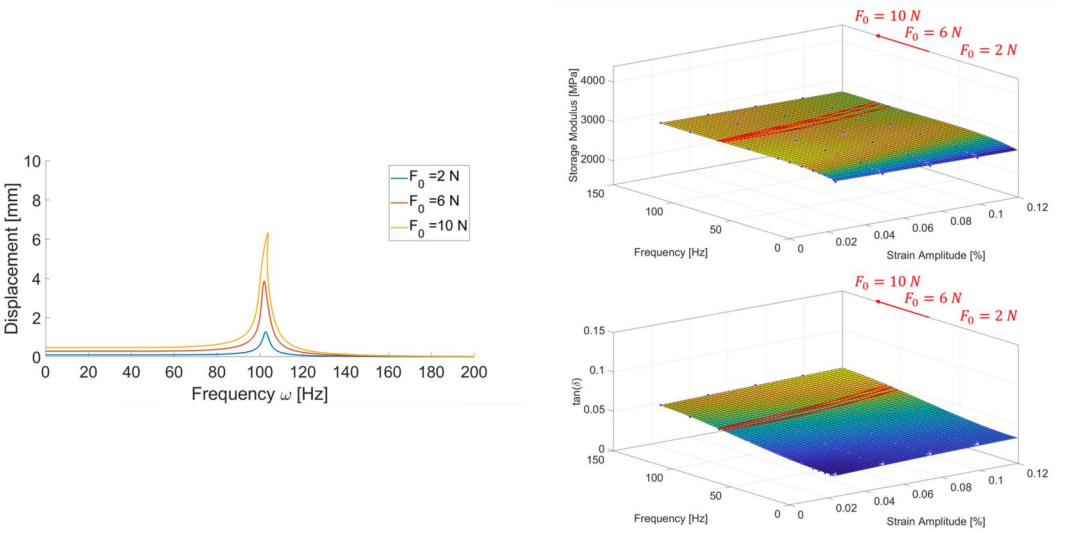

Figure 13. Frequency responses of the cantilever beam made of unreinforced epoxy (the red lines show the behavior of the dynamic mechanical properties at the resonant frequencies under the corresponding excitation force amplitudes for this sample).

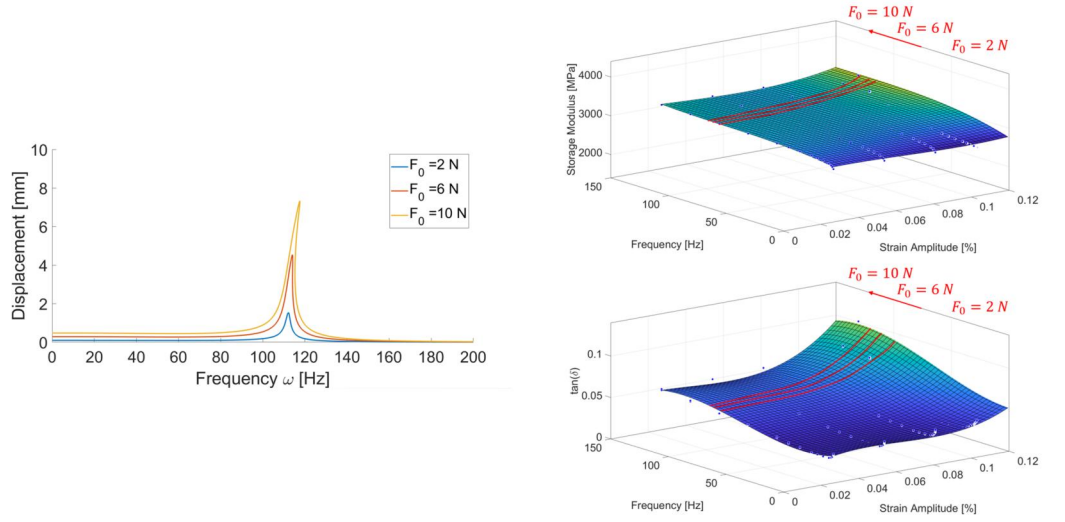

Figure 14. Frequency responses of the cantilever beam made of epoxy reinforced with FS for $m_f = 1\%$ (the red lines show the behavior of the dynamic mechanical properties at the resonant frequencies under the corresponding excitation force amplitudes for this sample).

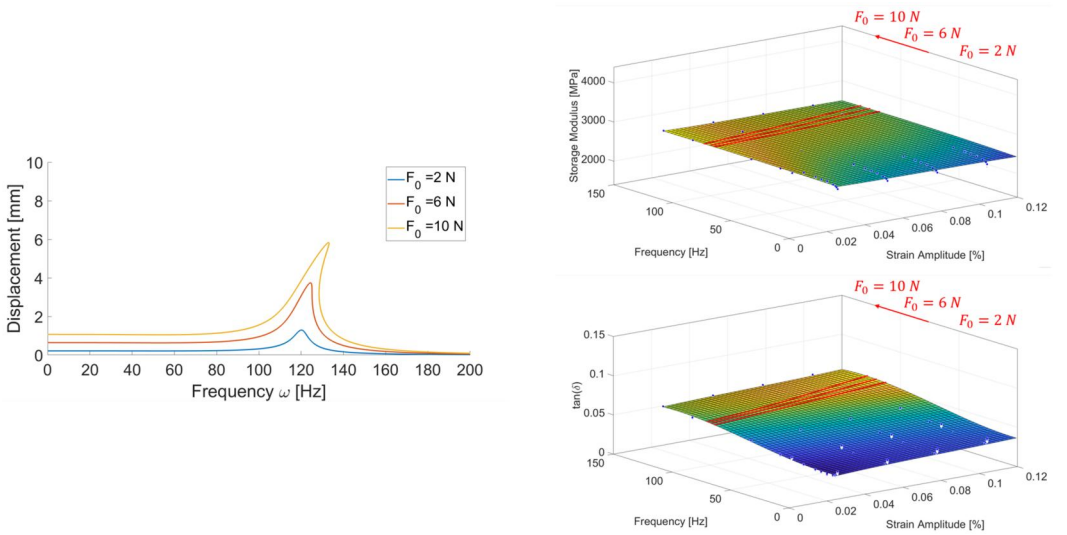

Figure 15. Frequency responses of the cantilever beam made of epoxy reinforced with HNT for $m_f = 1\%$ (the red lines show the behavior of the dynamic mechanical properties at the resonant frequencies under the corresponding excitation force amplitudes for this sample).

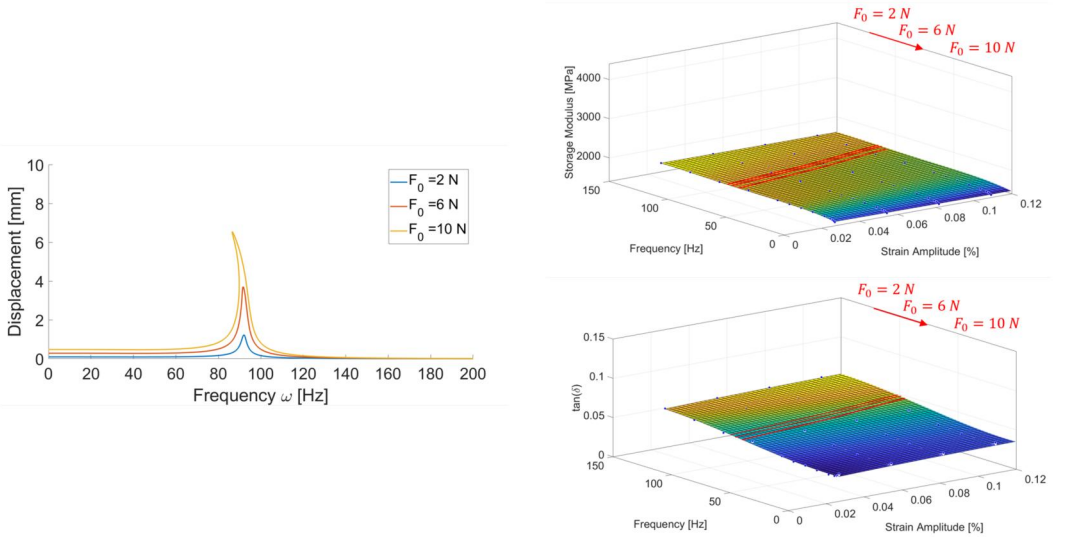

Figure 16. Frequency responses of the cantilever beam made of epoxy reinforced with rubber (Albipox 1000) for $m_f = 15\%$ (the red lines show the behavior of the dynamic mechanical properties at the resonant frequencies under the corresponding excitation force amplitudes for this sample).

sample under the corresponding excitation force amplitude is referred to as the" resonant frequency".

Figure 13 presents the frequency response functions (FRF) for the pure epoxy. The force amplitude changes from $2N$ to $10N$. It can be seen from Fig. 13, that for small force amplitude of $2N$, the response is linear. If the force amplitude increases, it shows slight softening. If the force amplitude reaches $10N$, there is hardening. This can be explained by the slight change in the storage modulus and the damping factor with strain amplitude and frequency as indicated in the surface plot in Fig. 13.

The FRF for a composite material which is epoxy reinforced with FS particles ($m_f = 1\%$), is shown in Fig. 14. The results suggest that adding FS particles into epoxy increase the natural frequency by about 10%. If the force amplitude on the composite material grow from $2N$ to $10N$, the vibration amplitude increases slightly and the composite material shows a stiffening behavior with strain amplitude and frequency. This can be explained with the appreciable rise of the storage modulus with increasing amplitude around the resonance frequency as marked in the plot (Fig. 14).

The FRF for HNT-reinforced composite material ($m_f = 1\%$) is given in Fig. 15. The data indicate that adding HNT particles into the epoxy considerably increases the natural frequency. Even for a smaller excitation force amplitude of $2N$, a significant nonlinearity (hardening effect) is observed. This can be explained by the changes in stiffness and a slight increase in damping with the addition of HNT. This hardening effect becomes much more significant when the excitation force amplitude is increased.

Figure 16 shows the FRF for a composite material which is epoxy reinforced with rubber (Albipox 1000) particles ($m_f = 15\%$). As shown in Fig. 16, adding rubber particles into epoxy decreases the natural frequency, as is expected. The force amplitude increases from $2N$ to $10N$. If the force amplitude on the composite material increases, the amplitude of the vibration also builds up and the softening effects become more noticeable. This softening can be explained with the slight drop in the storage modulus values with growing strain amplitudes around the resonance frequency as demonstrated in the surface plot in Fig. 16.

4.3. Discussion

After ensuring, through FTIR and SEM, the effects of manufacturing process on the mechanics of the composites are minimized, it is possible to relate the changes in the mechanical behavior of the materials solely to the reinforcing particles.

The results from the DMA tests and the numerical model of cantilever beam show significant differences in the behavior/performance of the nanocomposites reinforced with FS, HNT and rubber. The stress-strain plots, Fig. 8, highlight the hysteresis due to the intrinsic material properties related to the viscoelastic nature of the materials, thereby displaying and comparing the damping capabilities of plain epoxy and FS-reinforced epoxy.

Figure 9 shows the change of storage modulus of unreinforced epoxy, illustrating the sensitivity of this material to strain amplitude and excitation frequency. The inclusion of FS in epoxy, as shown in Fig. 10, leads to a rise in the storage modulus. The FS-reinforced samples proves the advantages of nanoreinforcements, especially in enhancing both stiffness and damping capabilities. Furthermore, the DMA tests on HNT-reinforced epoxy samples, presented in Fig. 11, suggest an enhancement in storage modulus and damping when HNT is introduced. It is observed that the stiffening effect of HNT is more significant compared to the stiffening effects of FS. Moreover, the data from the epoxy-based composites containing rubber particles suggest that, whilst these composites are more compliant, in other words, these composites have lower storage modulus overall, their behavior regarding frequency and strain amplitude is primarily consistent with other material groups. This is due to the behavior of epoxy predominantly governing the behavior of the composites.

The nonlinear behaviors are also observed through the numerical simulations, especially from the FRFs. The results of the numerical model point out to hardening and softening effects of different nanocomposites under varying force amplitudes. The cases of HNT-reinforced and rubber particle-reinforced epoxies, display strongly opposite behavior hinting toward the tailorability of the mechanical properties under external excitations with the selection of the appropriate nanofiller.

5. Conclusions

Within the scope of this study, different epoxy-based nanocomposites with FS, HNT and rubber nanoparticles are manufactured employing a consistent manufacturing procedure. The prepared nanocomposite specimens are characterized *via* FTIR analysis, SEM and DMA sweeping through frequency and amplitude. Following the characterization, a cantilever beam made of these manufactured nanocomposites is theoretically modeled, which displays the effects of the reinforcements on the dynamic mechanical characteristics of a simple mechanical structure/system. The beam is idealized to be an SDOF system, which is tuned for the fundamental natural frequency (first bending mode). The model is solved numerically using pseudo-arclength continuation technique.

The results of the FTIR reveal that there is no significant variation in chemical composition among the materials. Moreover, the SEM images acquired show that there are no major material flaws that might have affected the results of the mechanical characterization. The DMA tests demonstrate that the presence of various nanoreinforcements can significantly affect the storage modulus and the damping capabilities of the material. In terms of improving the stiffness and damping simultaneously, FS and HNT reinforcements have significant effects. The HNT-reinforced epoxies give well-improved results on stiffness and damping compared to the unreinforced epoxy.

Finally, the simulation of the cantilever beam shows the influence of the reinforcing particles on the dynamics of the beam by changing the material characteristics. The epoxy with rubber reinforcements show a reduction in resonant frequency. The HNT-reinforced epoxy displays significant stiffening nonlinearity as well as an increase in damping. This case study shows, that depending on the system requirements, modifying the material constituents with nanoparticles can have considerable effects on the overall dynamic behavior of a mechanical structure/system. For this reason, choosing the right nanofiller needs to be carefully considered, during the design of an engineering component.

The proposed method and the results obtained shed light on the considerable influence of nanoparticle reinforcements in changing the dynamic mechanical characteristics of epoxy-based nanocomposites. This integrated experimental and theoretical methodology can have impact on a broad spectrum of engineering for engineering design, particularly in areas where specific material behavior is important for performance. The results highlight the necessity of strategic selection of nanofillers, as they directly influence the stiffness, damping and therefore, the overall performance of composite materials. The in-depth experimental and simulation methodologies employed and proposed here bridge the gap of knowledge in understanding the interactions between nanoparticle type and the nonlinear behavior of epoxy nanocomposites. This study, therefore, serves as one of the earliest reference points for engineers and researchers to optimise/tailor the performance of composite materials for various applications.

This study also paves the way for future research, especially regarding nonlinear material behavior in polymer-based nanocomposites. Following this study, it would be interesting to consider other parameters in addition to amplitude and frequency of vibration to investigate the nonlinear nature of these epoxy-based nanocomposites such as the temperature and humidity as well as the effects of the combinations of multiple reinforcement types. Another aspect for research would be to study the effects of fatigue of such nanocomposites depending on the nanofillers.

Acknowledgments

Mertol Tüfekci would like to acknowledge the support of Scientific and Technological Research Council of Turkey (TUBITAK) (fund BİDEB 2213 2016/2) that makes this research possible. The authors also would like to thank Evonik for the courtesy of providing materials and Dr.Dr.-Ing. Stephan Sprenger for his helpful guidance. The authors would like to express gratitude to Dr. Ruth Brooker for her invaluable and helpful guidance on

experimental procedures and insightful advice throughout the research process. The authors would also like to acknowledge computational resources and support provided by the Imperial College Research Computing Service (http://doi.org/10.14469/hpc/2232).

Authors' contributions

- Mertol Tüfekci: Methodology, Formal analysis, Investigation, Software, Data curation, Writing-Original draft preparation.
- Tuğba Baytak: Formal analysis, Investigation.
- Osman Bulut: Formal analysis, Investigation.
- İnci Pir: Formal analysis, Investigation, Visualization, Data curation.
- Seren Acarer: Formal analysis, Investigation.
- Burak Özkal: Methodology, Investigation, Writing-Reviewing and Editing.
- Haibao Liu: Investigation, Writing-Reviewing and Editing.
- John P. Dear: Methodology, Writing-Reviewing and Editing, Supervision.
- Loic Salles: Methodology, Supervision.

References

Acarer, S., İ. Pir, M. Tüfekci, G. Türkoğlu Demirkol, and N. Tüfekci. 2021. "Manufacturing and Characterisation of Polymeric Membranes for Water Treatment and Numerical Investigation of Mechanics of Nanocomposite Membranes." *Polymers* 13 (10): 1661. https://doi.org/10.3390/polym13101661

Acarer, S., İnci Pir, M. Tüfekci, T. Erkoç, V. Öztekin, C. Dikicioğlu, G. T. Demirkol, et al. 2022. "Characterisation and Mechanical Modelling of Polyacrylonitrile-Based Nanocomposite Membranes Reinforced with Silica Nanoparticles." *Nanomaterials* 12 (21): 3721. https://doi.org/10.3390/nano12213721

Acarer, Seren, İnci Pir, Mertol Tüfekci, Tuğba Erkoç, Vehbi Öztekin, Sevgi Güneş Durak, Mehmet Şükrü Özçoban, et al. 2023. "Characterisation and Modelling the Mechanics of Cellulose Nanofibril Added Polyethersulfone Ultrafiltration Membranes." *Heliyon* 9 (2): e13086. https://doi.org/10.1016/j.heliyon.2023.e13086

Adhikari, S. 2000. "Damping Models for Structural Vibration." PhD thesis, Cambridge University Engineering Department, Cambridge, UK.

Adhikari, S., and B. Pascual. 2009. "Eigenvalues of Linear Viscoelastic Systems." *Journal of Sound and Vibration* 325 (4–5): 1000–1011. https://doi.org/10.1016/j.jsv.2009.04.008

Al-Furjan, M. S., B. Alzahrani, L. Shan, M. Habibi, and D. W. Jung. 2022. "Nonlinear Forced Vibrations of Nanocomposite-Reinforced Viscoelastic Thick Annular System under Hygrothermal Environment." *Mechanics Based Design of Structures and Machines* 50 (11): 4021–4047. https://doi.org/10.1080/15397734.2020.1824795

Amadori, S., and G. Catania. 2018. "An Effective Coating Material Solution and Modeling Technique for Damping Oriented Design of Thin Walled Mechanical Components." *Composite Structures* 191: 251–267. https://doi.org/10.1016/j.compstruct.2018.02.034

Banks, H. T., S. Hu, and Z. R. Kenz. 2011. "A Brief Review of Viscoelasticity." *Advances in Applied Mathematics and Mechanics* 3 (1): 1–51. https://doi.org/10.4208/aamm.10-m1030

Barot, T., D. Rawtani, and P. Kulkarni. 2020. "Physicochemical and Biological Assessment of Silver Nanoparticles Immobilized Halloysite Nanotubes-Based Resin Composite for Dental Applications." *Heliyon* 6 (3): e03601. https://doi.org/10.1016/j.heliyon.2020.e03601

Berahman, R., M. Raiati, M. Mehrabi Mazidi, and S. M. R. Paran. 2016. "Preparation and Characterization of Vulcanized Silicone Rubber/Halloysite Nanotube Nanocomposites: Effect of Matrix Hardness and HNT Content." *Materials & Design* 104: 333–345. https://doi.org/10.1016/j.matdes.2016.04.099

Bilasse, M., E. M. Daya, and L. Azrar. 2010. "Linear and Nonlinear Vibrations Analysis of Viscoelastic Sandwich Beams." *Journal of Sound and Vibration* 329 (23): 4950–4969. https://doi.org/10.1016/j.jsv.2010.06.012

Bouadi, H., and C. T. Sun. 1990. "Hygrothermal Effects on Structural Stiffness and Structural Damping of Laminated Composites." *Journal of Materials Science* 25 (1): 499–505. https://doi.org/10.1007/BF00714063

Chen, Z., T. Yu, Y. H. Kim, Z. Yang, and T. Yu. 2021. "Enhanced Dynamic Mechanical Properties of Different-Structured Nanoclays Incorporated BFRP Based on "Stick-Slip" Hypothesis." *Materials & Design* 207: 109870. https://doi.org/10.1016/j.matdes.2021.109870

Chung, D. D. 2001. "Review: Materials for Vibration Damping." *Journal of Materials Science* 36 (24): 5733–5737.

Crandall, S. H. 1970. "The Role of Damping in Vibration Theory." *Journal of Sound and Vibration* 11 (1): 3–IN1. https://doi.org/10.1016/S0022-460X(70)80105-5

Ebrahimi, F., A. Dabbagh, and A. Rastgoo. 2021. "Free Vibration Analysis of Multi-Scale Hybrid Nanocomposite Plates with Agglomerated Nanoparticles." *Mechanics Based Design of Structures and Machines* 49 (4): 487–510. https://doi.org/10.1080/15397734.2019.1692665

Ebrahimi, F., M. Nouraei, and A. Dabbagh. 2020. "Modeling Vibration Behavior of Embedded Graphene-Oxide Powder-Reinforced Nanocomposite Plates in Thermal Environment." *Mechanics Based Design of Structures and Machines* 48 (2): 217–240. https://doi.org/10.1080/15397734.2019.1660185

Esmaeeli, R., H. Aliniagerdroudbari, S. R. Hashemi, C. Jbr, and S. Farhad. 2019. "Designing a New Dynamic Mechanical Analysis (DMA) System for Testing Viscoelastic Materials at High Frequencies." *Modelling and Simulation in Engineering* 2019: 1–9. https://doi.org/10.1155/2019/7026267

Feng, J., and Z. Guo. 2016. "Temperature-Frequency-Dependent Mechanical Properties Model of Epoxy Resin and Its Composites." *Composites Part B: Engineering* 85: 161–169. https://doi.org/10.1016/j.compositesb.2015.09.040

Fuller, J., S. Mitchell, T. Pozegic, X. Wu, M. Longana, and M. Wisnom. 2021. "Experimental Evaluation of Hygrothermal Effects on Pseudo-Ductile Thin Ply Angle-Ply Carbon/Epoxy Laminates." *Composites Part B: Engineering* 227: 109388. https://doi.org/10.1016/j.compositesb.2021.109388

González, M. G., J. C. Cabanelas, and J. Baselga. 2012. "Applications of FTIR on Epoxy Resins - Identification, Monitoring the Curing Process, Phase Separation and Water Uptake." In *Infrared Spectroscopy - Materials Science, Engineering and Technology*, edited by Theophile Theophanides. London: Intech.

Hao, S., Z. Li, C. Yang, A. J. Marsden, I. A. Kinloch, and R. J. Young. 2022. "Interfacial Energy Dissipation in Bio-Inspired Graphene Nanocomposites." *Composites Science and Technology* 219: 109216. https://doi.org/10.1016/j.compscitech.2021.109216

Hu, X., and C. Zhou. 2022a. "Dynamic Analysis and Experiment of Quasi-Zero-Stiffness System with Nonlinear Hysteretic Damping." *Nonlinear Dynamics* 107 (3): 2153–2175. https://doi.org/10.1007/s11071-021-07136-1

Hu, X., and C. Zhou. 2022b. "The Effect of Various Damping on the Isolation Performance of Quasi-Zero-Stiffness System." *Mechanical Systems and Signal Processing* 171: 108944. https://doi.org/10.1016/j.ymssp.2022.108944

Jiang, Y., L. Li, and Y. Hu. 2023. "Strain Gradient Viscoelasticity Theory of Polymer Networks." *International Journal of Engineering Science* 192: 103937. https://doi.org/10.1016/j.ijengsci.2023.103937

Jin, X., J. Xu, Y. Pan, H. Wang, B. Ma, F. Liu, X. Yan, et al. 2022. "Lightweight and Multiscale Needle Quartz Fiber Felt Reinforced Siliconoxycarbide Modified Phenolic Aerogel Nanocomposite with Enhanced Mechanical, Insulative and Flame-Resistant Properties." *Composites Science and Technology* 217: 109100. https://doi.org/10.1016/j.compscitech.2021.109100

Johlitz, M., and S. Diebels. 2011. "Characterisation of a Polymer Using Biaxial Tension Tests. Part I: Hyperelasticity." *Archive of Applied Mechanics* 81 (10): 1333–1349. https://doi.org/10.1007/s00419-010-0480-1

Johnson, C. D., and D. A. Kienholz. 1982. "Finite Element Prediction of Damping in Structures with Constrained Viscoelastic Layers." *AIAA Journal* 20 (9): 1284–1290. https://doi.org/10.2514/3.51190

Jordan, J., K. I. Jacob, R. Tannenbaum, M. A. Sharaf, and I. Jasiuk. 2005. "Experimental Trends in Polymer Nanocomposites - A Review." *Materials Science and Engineering: A* 393 (1–2): 1–11. https://doi.org/10.1016/j.msea.2004.09.044

Jrad, H., J. L. Dion, F. Renaud, I. Tawfiq, and M. Haddar. 2013. "Experimental Characterization, Modeling and Parametric Identification of the Non Linear Dynamic Behavior of Viscoelastic Components." *European Journal of Mechanics - A/Solids* 42: 176–187. https://doi.org/10.1016/j.euromechsol.2013.05.004

Jrad, H., F. Renaud, J. L. Dion, I. Tawfiq, and M. Haddar. 2013. "Experimental Characterization, Modeling and Parametric Identification of the Hysteretic Friction Behavior of Viscoelastic Joints." *International Journal of Applied Mechanics* 05 (02): 1350018. https://doi.org/10.1142/S175882511350018X

Karkar, S., B. Cochelin, and C. Vergez. 2013. "A High-Order, Purely Frequency Based Harmonic Balance Formulation for Continuation of Periodic Solutions: The Case of Non-Polynomial Nonlinearities." *Journal of Sound and Vibration* 332 (4): 968–977. https://doi.org/10.1016/j.jsv.2012.09.033

Khaniki, H. B., and M. H. Ghayesh. 2023. "Highly Nonlinear Hyperelastic Shells: Statics and Dynamics." *International Journal of Engineering Science* 183: 103794. https://doi.org/10.1016/j.ijengsci.2022.103794
Khaniki, H. B., M. H. Ghayesh, and R. Chin. 2023a. "Theory and Experiment for Dynamics of Hyperelastic Plates with Modal Interactions." *International Journal of Engineering Science* 182: 103769. https://doi.org/10.1016/j.ijengsci.2022.103769
Khaniki, H. B., M. H. Ghayesh, R. Chin, and M. Amabili. 2022. "A Review on the Nonlinear Dynamics of Hyperelastic Structures." *Nonlinear Dynamics* 110 (2): 963–994. https://doi.org/10.1007/s11071-022-07700-3
Khaniki, H. B., M. H. Ghayesh, R. Chin, and S. Hussain. 2023b. "Internal Resonance and Bending Analysis of Thick Visco-Hyper-Elastic Arches." *Continuum Mechanics and Thermodynamics* 35 (1): 299–342. https://doi.org/10.1007/s00161-022-01166-9
Kim, B., J. Choi, S. Yang, S. Yu, and M. Cho. 2017. "Multiscale Modeling of Interphase in Crosslinked Epoxy Nanocomposites." *Composites Part B: Engineering* 120: 128–142. https://doi.org/10.1016/j.compositesb.2017.03.059
Kliem, M., J. Høgsberg, J. Vanwalleghem, A. Filippatos, S. Hoschützky, E. R. Fotsing, and C. Berggreen. 2019. "Damping Analysis of Cylindrical Composite Structures with Enhanced Viscoelastic Properties." *Applied Composite Materials* 26 (1): 85–113. https://doi.org/10.1007/s10443-018-9684-2
Krack, M., L. A. Bergman, and A. F. Vakakis. 2016. "On the Efficacy of Friction Damping in the Presence of Nonlinear Modal Interactions." *Journal of Sound and Vibration* 370: 209–220. https://doi.org/10.1016/j.jsv.2016.01.039
Krack, M., and J. Gross. 2019. Harmonic Balance for Nonlinear Vibration Problems. Cham: Springer.
Kuzielová, E., M. Slaný, M. Žemlička, J. Másilko, and M. T. Palou. 2021. "Phase Composition of Silica Fume—Portland Cement Systems Formed under Hydrothermal Curing Evaluated by FTIR, XRD, and TGA." *Materials* 14 (11): 2786. https://doi.org/10.3390/ma14112786
Lázaro, M., J. L. Pérez-Aparicio, and M. Epstein. 2012. "Computation of Eigenvalues in Proportionally Damped Viscoelastic Structures Based on the Fixed-Point Iteration." *Applied Mathematics and Computation* 219 (8): 3511–3529. https://doi.org/10.1016/j.amc.2012.09.026
Lee, C., X. Wei, J. W. Kysar, and J. Hone. 2008. "Measurement of the Elastic Properties and Intrinsic Strength of Monolayer Graphene." *Science* 321 (5887): 385–388. https://doi.org/10.1126/science.1157996
Li, C., C. Zhu, C. W. Lim, and S. Li. 2022. "Nonlinear in-Plane Thermal Buckling of Rotationally Restrained Functionally Graded Carbon Nanotube Reinforced Composite Shallow Arches under Uniform Radial Loading." *Applied Mathematics and Mechanics* 43 (12): 1821–1840. https://doi.org/10.1007/s10483-022-2917-7
Li, K. M., J. G. Jiang, S. C. Tian, X. J. Chen, and F. Yan. 2014. "Influence of Silica Types on Synthesis and Performance of Amine-Silica Hybrid Materials Used for CO_2 Capture." *The Journal of Physical Chemistry C* 118 (5): 2454–2462. https://doi.org/10.1021/jp408354r
Lin, R. M., and J. Zhu. 2009. "On the Relationship between Viscous and Hysteretic Damping Models and the Importance of Correct Interpretation for System Identification." *Journal of Sound and Vibration* 325 (1–2): 14–33. https://doi.org/10.1016/j.jsv.2009.02.051
Liu, Y., Y. Tang, P. Wang, and H. Zeng. 2019. "Carbonaceous Halloysite Nanotubes for the Stabilization of Co, Ni, Cu and Zn in River Sediments." *Environmental Science: Nano* 6 (8): 2420–2428. https://doi.org/10.1039/C9EN00326F
Lu, X., F. Detrez, J. Yvonnet, and J. Bai. 2021. "Identification of Elastic Properties of Interphase and Interface in Graphene-Polymer Nanocomposites by Atomistic Simulations." *Composites Science and Technology* 213: 108943. https://doi.org/10.1016/j.compscitech.2021.108943
Lu, X., R. Huang, H. Li, J. Long, and Z. Jiang. 2017. "Preparation of an Elastomer with Broad Damping Temperature Range Based on EPDM/ENR Blend." *Journal of Elastomers & Plastics* 49 (8): 758–773. https://doi.org/10.1177/0095244317698737
Ludwigson, M. N., R. S. Lakes, and C. C. Swan. 2002. "Damping and Stiffness of Particulate SiC-InSn Composite." *Journal of Composite Materials* 36 (19): 2245–2254. https://doi.org/10.1177/0021998302036019291
Luo, J. J., and I. M. Daniel. 2003. "Characterization and Modeling of Mechanical Behavior of Polymer/Clay Nanocomposites." *Composites Science and Technology* 63 (11): 1607–1616. https://doi.org/10.1016/S0266-3538(03)00060-5
Mace, T., J. Taylor, and C. W. Schwingshackl. 2020. "A Novel Technique to Extract the Modal Damping Properties of a Thin Blade." In *Conference Proceedings of the Society for Experimental Mechanics Series*, 247–250. New York: Springer.
Mace, T., J. Taylor, and C. W. Schwingshackl. 2022a. "Simplified Low Order Composite Laminate Damping Predictions via Multi-Layer Homogenisation." *Composites Part B: Engineering* 234: 109641. https://doi.org/10.1016/j.compositesb.2022.109641
Mace, T., J. Taylor, and C. W. Schwingshackl. 2022b. "Measurement of the Principal Damping Components of Composite Laminates." *Composite Structures* 302: 116199. https://doi.org/10.1016/j.compstruct.2022.116199

Maity, P., S. V. Kasisomayajula, V. Parameswaran, S. Basu, and N. Gupta. 2008. "Improvement in Surface Degradation Properties of Polymer Composites Due to Pre-Processed Nanometric Alumina Fillers." *IEEE Transactions on Dielectrics and Electrical Insulation* 15 (1): 63–72. https://doi.org/10.1109/T-DEI.2008.4446737
Nguyen, V. D., L. Wu, and L. Noels. 2019. "A Micro-Mechanical Model of Reinforced Polymer Failure with Length Scale Effects and Predictive Capabilities. Validation on Carbon Fiber Reinforced High-Crosslinked RTM6 Epoxy Resin." *Mechanics of Materials* 133: 193–213. https://doi.org/10.1016/j.mechmat.2019.02.017
Odent, J., J. M. Raquez, J. M. Thomassin, J. M. Gloaguen, F. Lauro, C. Jérôme, J. M. Lefebvre, and P. Dubois. 2015. "Mechanistic Insights on Nanosilica Self-Networking Inducing Ultra-Toughness of Rubber-Modified Polylactide-Based Materials." *Nanocomposites* 1 (3): 113–125. https://doi.org/10.1179/2055033215Y.0000000005
Ogden, R. 1984. *Non-Linear Elastic Deformations*. Vol. 1. New York: E. Horwood.
Ouis, D. 2004. "Characterization of Polymers by Means of a Standard Viscoelastic Model and Fractional Derivate Calculus." *International Journal of Polymeric Materials* 53 (8): 633–644. https://doi.org/10.1080/009114030490472845
Owais, M., J. Zhao, A. Imani, G. Wang, H. Zhang, and Z. Zhang. 2019. "Synergetic Effect of Hybrid Fillers of Boron Nitride, Graphene Nanoplatelets, and Short Carbon Fibers for Enhanced Thermal Conductivity and Electrical Resistivity of Epoxy Nanocomposites." *Composites Part A: Applied Science and Manufacturing* 117: 11–22. https://doi.org/10.1016/j.compositesa.2018.11.006
Ozdemir, N. G., T. Zhang, I. Aspin, F. Scarpa, H. Hadavinia, and Y. Song. 2016. "Toughening of Carbon Fibre Reinforced Polymer Composites with Rubber Nanoparticles for Advanced Industrial Applications." *Express Polymer Letters* 10 (5): 394–407. https://doi.org/10.3144/expresspolymlett.2016.37
Padovan, J., and J. T. Sawicki. 1998. "Nonlinear Vibrations of Fractionally Damped Systems." *Nonlinear Dynamics* 16 (4): 321–336. https://doi.org/10.1023/A:1008289024058
Parveen, S., S. Pichandi, P. Goswami, and S. Rana. 2020. "Novel Glass Fibre Reinforced Hierarchical Composites with Improved Interfacial, Mechanical and Dynamic Mechanical Properties Developed Using Cellulose Microcrystals." *Materials & Design* 188: 108448. https://doi.org/10.1016/j.matdes.2019.108448
Pierro, E., and G. Carbone. 2021. "A New Technique for the Characterization of Viscoelastic Materials: Theory, Experiments and Comparison with DMA." *Journal of Sound and Vibration* 515: 116462. https://doi.org/10.1016/j.jsv.2021.116462
Rathi, A., S. Kundalwal, S. Singh, and A. Kumar. 2021. "Adhesive and Viscoelastic Response of Mwcnt/zro2 Hybrid Epoxy Nanocomposites." *Journal of Mechanics of Materials and Structures* 16 (3): 281–292. https://doi.org/10.2140/jomms.2021.16.281
Richards, A. W., and G. M. Odegard. 2010. "Constitutive Modeling of Electrostrictive Polymers Using a Hyperelasticity-Based Approach." *Journal of Applied Mechanics* 77 (1): 1–5. https://doi.org/10.1115/1.3173766
Rossikhin, Y. A., and M. V. Shitikova. 1997. "Application of Fractional Derivatives to the Analysis of Damped Vibrations of Viscoelastic Single Mass Systems." *Acta Mechanica* 120 (1–4): 109–125. https://doi.org/10.1007/BF01174319
Sadd, M. H. 2019. *Continuum Mechanics Modeling of Material Behavior*. Amsterdam: Elsevier.
Sadjadi, S., M. M. Heravi, and M. Daraie. 2017. "Heteropolyacid Supported on Amine-Functionalized Halloysite Nano Clay as an Efficient Catalyst for the Synthesis of Pyrazolopyranopyrimidines via Four-Component Domino Reaction." *Research on Chemical Intermediates* 43 (4): 2201–2214. https://doi.org/10.1007/s11164-016-2756-8
Schapery, R. A. 1969. "On the Characterization of Nonlinear Viscoelastic Materials." *Polymer Engineering & Science* 9 (4): 295–310. https://doi.org/10.1002/pen.760090410
Shokri, B., M. A. Firouzjah, and S. I. Hosseini. 2009. "FTIR Analysis of Silicon Dioxide Thin Film Deposited by Metal Organic-Based PECVD." Proceedings of 19th International Plasma Chemistry Society, 1–4.
Sierra-Romero, A., and B. Chen. 2018. "Strategies for the Preparation of Polymer Composites with Complex Alignment of the Dispersed Phase." *Nanocomposites* 4 (4): 137–155. https://doi.org/10.1080/20550324.2018.1551830
Singh Kashyap, V., U. Agrawal, K. Arora, and G. Sancheti. 2021. "FTIR Analysis of Nanomodified Cement Concrete Incorporating Nano Silica and Waste Marble Dust." *IOP Conference Series: Earth and Environmental Science* 796 (1): 012022. https://doi.org/10.1088/1755-1315/796/1/012022
Sprenger, S. 2020. "Nanosilica-Toughened Epoxy Resins." *Polymers* 12 (8): 1777. https://doi.org/10.3390/polym12081777
Stanley, W. F., A. K. Bandaru, S. Rana, S. Parveen, and S. Pichandi. 2021. "Mechanical, Dynamic-Mechanical and Wear Performance of Novel Non-Crimp Glass Fabric-Reinforced Liquid Thermoplastic Composites Filled with Cellulose Microcrystals." *Materials & Design* 212: 110276. https://doi.org/10.1016/j.matdes.2021.110276
Tan, X., and R. J. Rogers. 1995. "Equivalent Viscous Damping Models of Coulomb Friction in Multi-Degree-of-Freedom Vibration Systems." *Journal of Sound and Vibration* 185 (1): 33–50. https://doi.org/10.1006/jsvi.1994.0362
Thostenson, E. T., C. Li, and T. W. Chou. 2005. "Nanocomposites in Context." *Composites Science and Technology* 65 (3–4): 491–516. https://doi.org/10.1016/j.compscitech.2004.11.003
Torvik, P. J., and R. L. Bagley. 1984. "On the Appearance of the Fractional Derivative in the Behavior of Real Materials." *Journal of Applied Mechanics* 51 (2): 294–298. https://doi.org/10.1115/1.3167615
Tüfekci, E. 2001. "Exact Solution of Free in-Plane Vibration of Shallow Circular Arches." *International Journal of Structural Stability and Dynamics* 01: 409–428.

Tüfekci, M., B. Özkal, C. Maharaj, H. Liu, J. P. Dear, and L. Salles. 2023. "Strain-Rate-Dependent Mechanics and Impact Performance of Epoxy-Based Nanocomposites." *Composites Science and Technology* 233: 109870. https://doi.org/10.1016/j.compscitech.2022.109870
Tüfekci, M., Ö. E. Genel, A. Tatar, and E. Tüfekci. 2020. "Dynamic Analysis of Composite Wind Turbine Blades as Beams: An Analytical and Numerical Study." *Vibration* 4 (1): 1–15. https://doi.org/10.3390/vibration4010001
Tufekci, M., S. Gunes-Durak, T. Ormanci-Acar, and N. Tufekci. 2019. "Effects of Geometry and PVP Addition on Mechanical Behavior of Pei Membranes for Use in Wastewater Treatment." *Journal of Applied Polymer Science* 136 (7): 47073. https://doi.org/10.1002/app.47073
Tüfekci, M., T. Mace, B. Özkal, J. P. Dear, C. W. Schwingshackl, and L. Salles. 2021. "Dynamic Behaviour of a Nanocomposite: Epoxy Reinforced with Fumed Silica Nanoparticles." XXV ICTAM, Milano.
Vescovini, R., and C. Bisagni. 2015. "A Procedure for the Evaluation of Damping Effects in Composite Laminated Structures." *Progress in Aerospace Sciences* 78: 19–29. https://doi.org/10.1016/j.paerosci.2015.05.004
Wang, X., J. Zhang, Z. Wang, S. Zhou, and X. Sun. 2011. "Effects of Interphase Properties in Unidirectional Fiber Reinforced Composite Materials." *Materials & Design* 32 (6): 3486–3492. https://doi.org/10.1016/j.matdes.2011.01.029
Woodhouse, J. 1998. "Linear Damping Models for Structural Vibration." Journal of *Sound and Vibration* 215: 547–569.
Xiao, Z., X. Jing, and L. Cheng. 2013. "The Transmissibility of Vibration Isolators with Cubic Nonlinear Damping under Both Force and Base Excitations." *Journal of Sound and Vibration* 332 (5): 1335–1354. https://doi.org/10.1016/j.jsv.2012.11.001
Xu, C., and L. Li. 2023. "A Surpassingly Stiff yet Lossy Multiscale Nanocomposite Inspired by Bio-Architecture." *Materials Today Communications* 35: 105982. https://doi.org/10.1016/j.mtcomm.2023.105982
Xu, X., and N. Gupta. 2018. "Determining Elastic Modulus from Dynamic Mechanical Analysis Data: Reduction in Experiments Using Adaptive Surrogate Modeling Based Transform." *Polymer* 157: 166–171. https://doi.org/10.1016/j.polymer.2018.10.036
Xu, X., C. Koomson, M. Doddamani, R. K. Behera, and N. Gupta. 2019. "Extracting Elastic Modulus at Different Strain Rates and Temperatures from Dynamic Mechanical Analysis Data: A Study on Nanocomposites." *Composites Part B: Engineering* 159: 346–354. https://doi.org/10.1016/j.compositesb.2018.10.015

Appendix A: Dynamic mechanical analysis: loss modulus results

Here, the loss factor of the manufactured materials is presented in Figures A1–A3 for completeness.

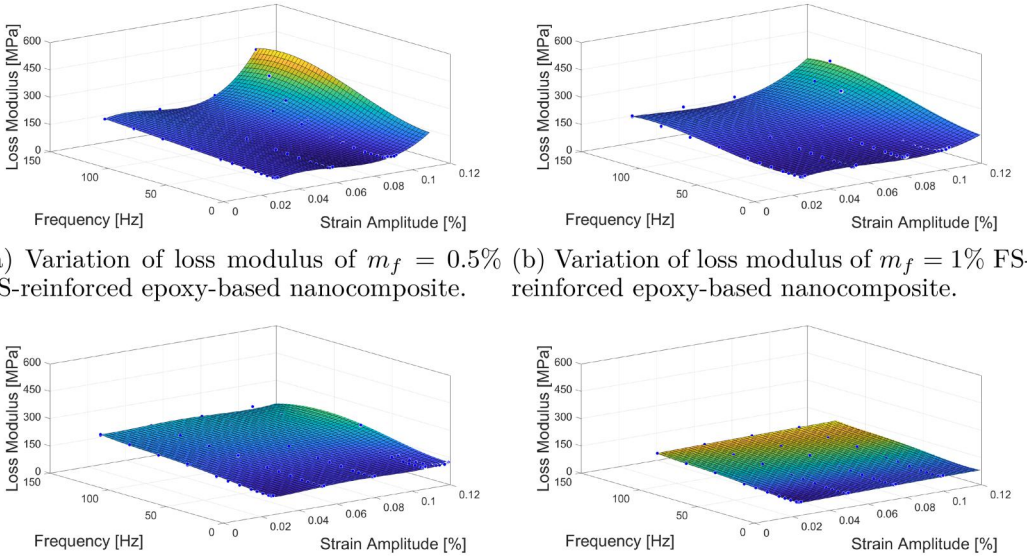

(a) Variation of loss modulus of $m_f = 0.5\%$ FS-reinforced epoxy-based nanocomposite.

(b) Variation of loss modulus of $m_f = 1\%$ FS-reinforced epoxy-based nanocomposite.

(c) Variation of loss modulus of $m_f = 1.5\%$ FS-reinforced epoxy-based nanocomposite.

(d) Variation of loss modulus of $m_f = 2\%$ FS-reinforced epoxy-based nanocomposite.

Figure A1. Variation of loss modulus of FS-reinforced epoxy with strain amplitude (up to 0.12%) and frequency (up to 150 Hz).

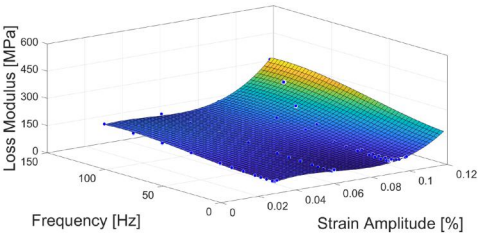

(a) Variation of loss modulus of $m_f = 0.5\%$ HNT-reinforced epoxy-based nanocomposite.

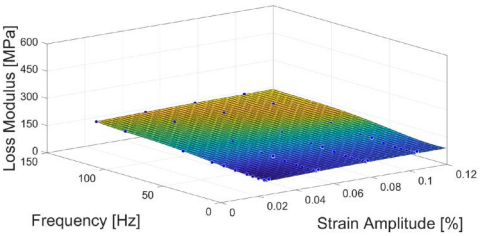

(b) Variation of loss modulus of $m_f = 1\%$ HNT-reinforced epoxy-based nanocomposite.

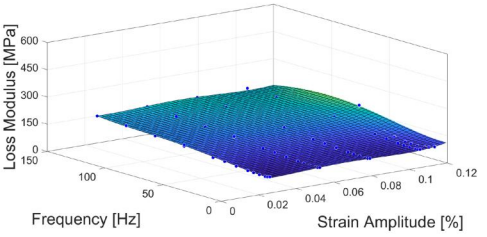

(c) Variation of loss modulus of $m_f = 1.5\%$ HNT-reinforced epoxy-based nanocomposite.

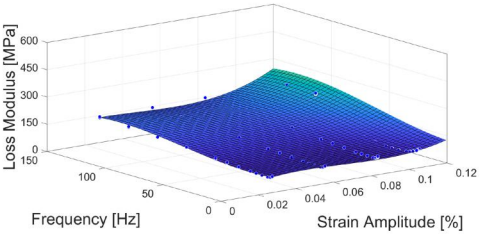

(d) Variation of loss modulus of $m_f = 2\%$ HNT-reinforced epoxy-based nanocomposite.

Figure A2. Variation of loss modulus of HNT-reinforced epoxy with strain amplitude (up to 0.12%) and frequency (up to 150 Hz).

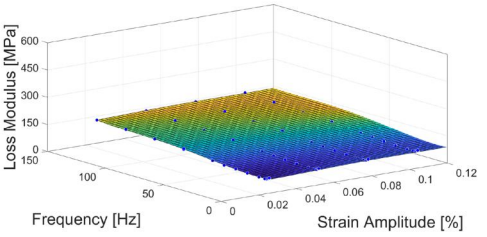

(a) Variation of loss modulus of $m_f = 5\%$ rubber (Albipox 1000)-reinforced epoxy-based nanocomposite.

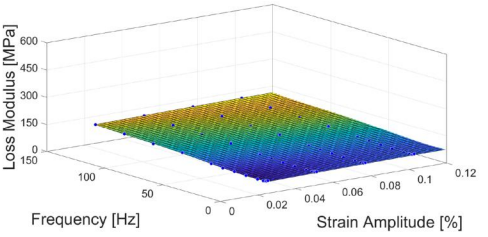

(b) Variation of loss modulus of $m_f = 10\%$ rubber (Albipox 1000)-reinforced epoxy-based nanocomposite.

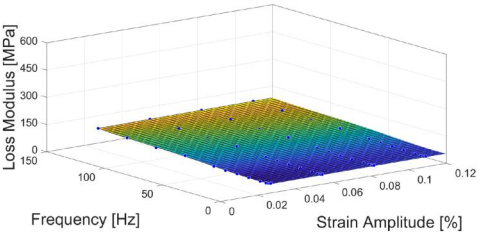

(c) Variation of loss modulus of $m_f = 15\%$ rubber (Albipox 1000)-reinforced epoxy-based nanocomposite.

Figure A3. Variation of loss modulus of rubber (Albipox 1000)-reinforced epoxy with strain amplitude (up to 0.12%) and frequency (up to 150 Hz).